

A poroplastic model of structural reorganisation in porous media of biomechanical interest

Original

A poroplastic model of structural reorganisation in porous media of biomechanical interest / Grillo, A., Prohl, R., Wittum, G.. - In: CONTINUUM MECHANICS AND THERMODYNAMICS. - ISSN 0935-1175. - STAMPA. - 28:(2016), pp. 579-601. [10.1007/s00161-015-0465-y]

Availability:

This version is available at: 11583/2627606 since: 2020-06-02T12:11:04Z

Publisher:

Springer

Published

DOI:10.1007/s00161-015-0465-y

Terms of use:

This article is made available under terms and conditions as specified in the corresponding bibliographic description in the repository

Publisher copyright

Springer postprint/Author's Accepted Manuscript

This version of the article has been accepted for publication, after peer review (when applicable) and is subject to Springer Nature's AM terms of use, but is not the Version of Record and does not reflect post-acceptance improvements, or any corrections. The Version of Record is available online at: <http://dx.doi.org/10.1007/s00161-015-0465-y>

(Article begins on next page)

A poroplastic model of structural reorganisation in porous media of biomechanical interest

Dedicated to Prof. David Steigmann in recognition of his contributions

Alfio Grillo · Raphael Prohl ·
Gabriel Wittum

Received: date / Accepted: date

DOI: 10.1007/s00161-015-0465-y. Available online: August 13, 2015
Journal: *Continuum Mechanics and Thermodynamics* (Springer)

1 **Abstract** We present a poroplastic model of structural reorganisation in a
2 binary mixture comprising a solid and a fluid phase. The solid phase is the
3 macroscopic representation of a deformable porous medium, which exemplifies
4 the matrix of a biological system (consisting e.g. of cells, extra-cellular matrix,
5 collagen fibres). The fluid occupies the interstices of the porous medium and
6 is allowed to move throughout it. The system reorganises its internal structure
7 in response to mechanical stimuli. Such structural reorganisation, referred to
8 as *remodelling*, is described in terms of “plastic” distortions, whose evolution
9 is assumed to obey a phenomenological flow rule driven by stress. We study
10 the influence of remodelling on the mechanical and hydraulic behaviour of
11 the system, showing how the plastic distortions modulate the flow pattern of
12 the fluid, and the distributions of pressure and stress inside it. To accomplish
13 this task, we solve a highly non-linear set of model equations by elaborating
14 a previously developed numerical procedure, which is implemented in a non-
15 commercial Finite Element solver.

A. Grillo
DISMA “G.L. Lagrange”, Politecnico di Torino, C.so Duca degli Abruzzi 24, I-10129, Torino
(TO) Italy
Tel.: +39-011-0907531
Fax: +39-011-0907599
E-mail: alfio.grillo@polito.it

R. Prohl
Steinbeis Center, Simulation in Technology, Bussardweg 6, D-75446 Wiernsheim, Germany.
E-mail: raphael@techsim.org

G. Wittum
G-CSC, Goethe Universität Frankfurt. Kettenhofweg 139, D-60325, Frankfurt am Main,
Germany. E-mail: wittum@gcsc.uni-frankfurt.de

16 **Keywords** Mixture Theories · Porous Media · Poroplasticity · Remodelling ·
17 Soft Tissues

18 **1 Introduction**

19 The remodelling, or structural reorganisation, of a biological system might
20 be defined as the result of an *ensemble* of processes that concur to adapt its
21 structure and material properties to both internal and external stimuli. In
22 addition to remodelling, a biological system may also experience growth, i.e.,
23 it may gain or lose mass. Growth can be appositional or volumetric. In the
24 first case, new material is either removed or laid over the pre-existing one [12].
25 In the second case, instead, the variation of mass can be diverted either in a
26 change of volume or in a change of density of the system [31, 62, 63].

27 In principle, a comprehensive study of growth and remodelling requires an
28 interdisciplinary approach, in which genetic aspects and molecular processes
29 as well as intracellular and intercellular activities are accounted for. Further-
30 more, a thorough analysis of the functioning of biological systems calls for
31 multi-scale and multi-level mathematical models, which should couple chem-
32 ical, electrical, and mechanical phenomena. Despite these intricacies, some
33 essential features of the evolution of biological systems can be captured by
34 purely mechanical theories of growth and remodelling. For a given biological
35 system, the starring characters of such theories are the parameters describing
36 its kinematics and structural evolution, and the generalised forces conjugate
37 with the selected parameters. Within a purely mechanical approach, several
38 problems of growth and remodelling can be studied. Growth, in general, con-
39 tributes to change the properties and internal structure of the tissue in which it
40 occurs. A relevant aspect of this phenomenology is that grown tissues usually
41 feature residual stresses, which means that, even though a grown tissue finds
42 itself in an unloaded configuration, it is not necessarily in a stress-free state.
43 For example, this is true for arteries [52]. Thus, as suggested in [90], growth
44 can be thought of as the process that brings the tissue from a zero-stress state
45 to a state in which residual stresses may be present even in the absence of
46 external loading. As is well-known, the stress-free state of a body (which is
47 also referred to as “the natural state”) is not a true configuration. Rather,
48 it is a collection of relaxed body pieces, which cannot be attained by simply
49 deforming the body. Consequently, growth cannot be described just in terms
50 of deformation, deformation gradients, and the related measures of stress. In
51 fact, one has to introduce also the concept of incompatible distortions in order
52 to account for the transformation connecting the natural state of a tissue with
53 the unloaded—yet not stress-free—configuration chosen as reference. The dis-
54 tortions due to growth are generally non-integrable and incompatible. They
55 are said to be non-integrable when they cannot be expressed as deformation
56 gradients, and are said to be incompatible when they lead to the loss of flat-
57 ness of the body manifold [72]. Moreover, distortions are both formally and
58 conceptually distinct from deformations, which describe the global change of

59 shape of the tissue. To account for distortions, Rodriguez et al. [90] invoked
60 the Bilby-Kröner-Lee (BKL) decomposition of the deformation gradient tensor,
61 thereby separating the “elastic” part of the overall deformation from the
62 “anelastic” one, which is related to growth and remodelling, and need not be
63 compatible.

64 The use of the BKL decomposition permits to exploit several analogies with
65 the theory of Elastoplasticity. For example, in a general model of growth, the
66 anelastic distortions associated with the structural reorganisation of a tissue
67 were described in terms of material inhomogeneities in [31], while the concept
68 of “evolving natural configurations” [89] was used for modelling tumour growth
69 both in monophasic and in multiphasic materials [1, 86].

70 In this paper, we focus on remodelling only. This can be done because there
71 exist remodelling processes that do not lead to variations of mass. Moreover,
72 there exist cases in which remodelling takes place over time-scales that are
73 well-separated from those characterising growth, and can be thus decoupled
74 from the growth-driven evolution of the system under study. For example,
75 these conditions are met in cellular aggregates and in tumour spheroids, when
76 their remodelling consists of the reorganisation of the adhesion bonds among
77 the cells [42]. This kind of remodelling can be described by hypothesising
78 that the considered biological systems exhibit elastoplastic behaviour [4] (or,
79 in some cases, elasto-visco-plastic behaviour [84]), and assuming that plastic
80 distortions arise when the stress in the system exceeds a given threshold [42].
81 The closeness of the present setting with the classical theory of Elastoplasticity
82 (cf. e.g. [65, 71]) makes it rather natural to employ the BKL decomposition in
83 order to define a stress-free state for the system, and separate the plastic
84 distortions due to remodelling from the elastic part of the overall deformation
85 gradient. Moreover, as is the case in Elastoplasticity, also in this framework
86 the plastic distortions are generally non-integrable and incompatible. For this
87 reason, when referring to the distortions associated with the evolution of the
88 internal structure of a body (i.e., with the process of remodelling), we shall
89 use the adjectives “anelastic” and “plastic” interchangeably.

90 Following [3, 45], we consider a biphasic mixture comprising a solid and
91 a fluid phase, and take it as an exemplification of a biological system. We
92 study the evolution of the mixture in response to external loads by prescribing
93 that, under suitable conditions, a remodelling process of the solid phase
94 occurs. To accomplish this task, we formulate a finite-deformation poroplastic
95 model of the mixture, which is able to determine the deformation of the solid
96 phase, the velocity of the fluid phase, and the plastic distortions associated
97 with the occurrence of remodelling. To solve the problem, we elaborate a computational
98 algorithm that aims at generalising a well-established numerical
99 procedure—the Return Mapping Algorithm (RMA)—to a class of anelastic
100 models not necessarily complying with all the hypotheses on which the RMA
101 is based [93]. Besides testing the proposed algorithm, our main purpose is to
102 evaluate the influence of remodelling on the fluid velocity, overall deformation,
103 and distributions of pressure and constitutive stress in the system under study.

We remark that mixture theory has been largely employed in modelling biomechanical problems of different kind. These range from tumour growth [2], in which the considered mixture consists of a fluid and one or more cell populations, to bone reconstruction [60], in which the mixture consists of the bone itself and some grafted bio-resorbable material.

The issue of structural reorganisation is largely investigated in the context of bone biomechanics, and has recently contributed also to raise questions in the field of optimal control theory. For example, optimal control procedures have been elaborated in [5] for assessing the structural efficiency of adaptive materials, and in [6] for studying the adaptation of bones under mechanical stimuli. They have also been used for modelling the trabecular architecture of bones [7], and for evaluating the bone density distribution [8]. Another problem connected with bone remodelling, which concerns the interaction of bone with resorbable biomaterial, has been addressed in [9–11].

The paper is organised as follows. In Sect. 2, we review some aspects of the theory of biphasic mixtures, and introduce the BKL decomposition in the framework of porous media. In Sect. 3, we establish the constitutive framework, study dissipation, and determine the evolution law for remodelling. In Sect. 4, we describe the numerical procedure elaborated for solving the model equations. In Sect. 5, we present and discuss the obtained results. Finally, in section 6, we outline some critical remarks on the employed model, and propose some plans for future research.

2 Theoretical background

For our purposes, we consider a binary system comprising a porous solid medium, also referred to as “matrix” hereafter, and a fluid. The region of space occupied by the system as a whole can be partitioned into two complementary sub-regions. One of these regions is occupied by the solid particles constituting the matrix, while the other one, which is generated by the voids of the matrix, is assumed to be filled with the fluid. If the latter sub-region is connected in topological sense, it is termed “pore space”, and the fluid can circulate throughout it. In the following, the matrix and the fluid shall also be called “phases”. At a sufficiently coarse scale of observation, the system can be viewed as a biphasic mixture, which means that both the matrix and the fluid are admitted to co-exist at each point of space occupied by the system. Note that there may be cases in which the connectedness of the void region is not granted. This happens, e.g., in solid bodies with micro-periodic non-connected inclusions filled with fluid [26].

2.1 Kinematics of biphasic mixtures

We base the forthcoming description of the kinematics of biphasic mixtures on the theory developed in [87, 88], and recently summarised in [94]. We denote by

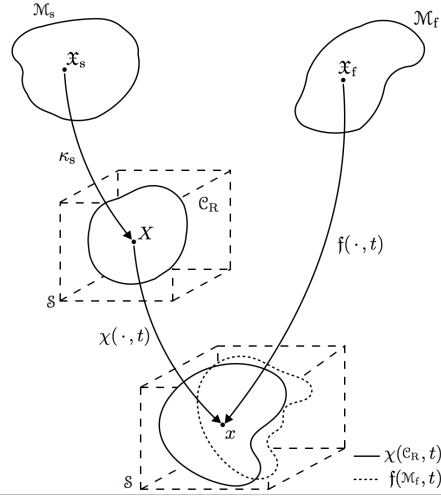


Fig. 1 Graphical representation of the kinematics of biphasic mixtures. Picture redrawn and adapted from [88]

144 \mathcal{M}_s and \mathcal{M}_f the two smooth three-dimensional material manifolds associated
 145 with the matrix and the fluid, respectively. The manifold \mathcal{M}_s is embedded
 146 into the three-dimensional Euclidean point space \mathcal{S} by means of the smooth
 147 localisation function $\kappa_s: \mathcal{M}_s \rightarrow \mathcal{S}$, such that, for every solid particle $\mathfrak{X}_s \in \mathcal{M}_s$,
 148 there exists a reference placement $X = \kappa_s(\mathfrak{X}_s) \in \mathcal{S}$. The set $\mathcal{C}_R = \kappa_s(\mathcal{M}_s)$ is
 149 chosen as the reference configuration for the mixture. The motion of the solid
 150 constituent is the one-parameter family of smooth mappings $\chi(\cdot, t): \mathcal{C}_R \rightarrow \mathcal{S}$,
 151 where $t \in \mathcal{J} \subseteq \mathbb{R}$ is time and \mathcal{J} is the interval of time over which the mixture
 152 is observed. The set $\chi(\mathcal{C}_R, t) \subset \mathcal{S}$ defines the current configuration of the solid
 153 phase. Each point $x \in \chi(\mathcal{C}_R, t) \subset \mathcal{S}$ is such that $x = \chi(X, t)$, with $X \in \mathcal{C}_R$
 154 and $t \in \mathcal{J}$. Similarly, the motion of the fluid is defined by $\mathfrak{f}(\cdot, t): \mathcal{M}_f \rightarrow \mathcal{S}$,
 155 with $t \in \mathcal{J}$. The map $\mathfrak{f}(\cdot, t)$ places a fluid particle $\mathfrak{X}_f \in \mathcal{M}_f$ in the spatial point
 156 $x = \mathfrak{f}(\mathfrak{X}_f, t) \in \mathfrak{f}(\mathcal{M}_f, t)$, where $\mathfrak{f}(\mathcal{M}_f, t)$ is the region of \mathcal{S} occupied by the fluid at
 157 time t . Therefore, at the same instant of time, the biphasic mixture occupies
 158 the set $\mathcal{C}_t = \chi(\kappa_s(\mathcal{M}_s), t) \cap \mathfrak{f}(\mathcal{M}_f, t) \subset \mathcal{S}$. By construction, solid and fluid
 159 particles co-exist at each point $x \in \mathcal{C}_t$. A schematic picture of the kinematics
 160 of biphasic mixtures is reported in Fig. 1, which has been adapted from [88].

161 We introduce the tangent spaces attached at $x \in \mathcal{S}$ and $X \in \mathcal{C}_R$, i.e., $T_x \mathcal{S}$ and
 162 $T_X \mathcal{C}_R$, the tangent bundles $T\mathcal{S} := \sqcup_{x \in \mathcal{S}} T_x \mathcal{S}$ and $T\mathcal{C}_R = \sqcup_{X \in \mathcal{C}_R} T_X \mathcal{C}_R$ (where
 163 \sqcup stands for “disjoint union” of sets), and their dual spaces $T^* \mathcal{S}$ and $T^* \mathcal{C}_R$,
 164 termed cotangent bundles. In addition, for any pair of natural numbers $r \geq 0$

165 and $s \geq 0$, we define the spaces [33]

$$[T\mathcal{S}]_s^r = \underbrace{T\mathcal{S} \otimes \dots \otimes T\mathcal{S}}_{r \text{ times}} \otimes \underbrace{T^*\mathcal{S} \otimes \dots \otimes T^*\mathcal{S}}_{s \text{ times}}, \quad (1a)$$

$$[T\mathcal{C}_R]_s^r = \underbrace{T\mathcal{C}_R \otimes \dots \otimes T\mathcal{C}_R}_{r \text{ times}} \otimes \underbrace{T^*\mathcal{C}_R \otimes \dots \otimes T^*\mathcal{C}_R}_{s \text{ times}}. \quad (1b)$$

166 When r is zero, we simply write $[T\mathcal{S}]_s^0$ and $[T\mathcal{C}_R]_s^0$. Analogously, when s is zero,
 167 we adopt the notation $[T\mathcal{S}]_0^r$ and $[T\mathcal{C}_R]_0^r$. For the sake of generality, we adopt
 168 the covariant formalism [68]. In the forthcoming calculations, we employ the
 169 spatial metric tensor, $\mathbf{g} \in [T\mathcal{S}]_2^0$, and the “material” metric tensor, $\mathbf{G} \in [T\mathcal{C}_R]_2^0$.
 170 Moreover, we adhere to the convention that the gradient of scalar fields returns
 171 a covector, and that all the stress tensors introduced in the following have
 172 contravariant components in their component representation.

173 The velocity of a solid particle, \mathfrak{X}_s , passing through $x = \chi(\kappa_s(\mathfrak{X}_s), t)$ at
 174 time t is denoted by $\mathbf{v}_s(x, t) = \dot{\chi}(\kappa_s(\mathfrak{X}_s), t) = \dot{\chi}(X, t) \in T_x\mathcal{S}$. Analogously,
 175 $\mathbf{v}_f(x, t) = \dot{\mathfrak{f}}(\mathfrak{X}_f, t) \in T_x\mathcal{S}$ is the spatial velocity of a fluid particle, \mathfrak{X}_f , passing
 176 through $x = \mathfrak{f}(\mathfrak{X}_f, t)$. The velocity of the fluid relative to the solid is given by
 177 $\mathbf{v}_{fs}(x, t) = \mathbf{v}_f(x, t) - \mathbf{v}_s(x, t)$, with $x = \chi(\kappa_s(\mathfrak{X}_s), t) = \mathfrak{f}(\mathfrak{X}_f, t)$. Moreover, the
 178 acceleration of the α th phase is defined by $\mathbf{a}_\alpha(x, t) = D_\alpha \mathbf{v}_\alpha(x, t)$, where D_α
 179 is the substantial derivative operator with respect to \mathbf{v}_α , i.e.,

$$D_\alpha \mathbf{v}_\alpha = \partial_t \mathbf{v}_\alpha + (\text{grad } \mathbf{v}_\alpha) \mathbf{v}_\alpha, \quad \alpha = s, f. \quad (2)$$

180 To express the velocity of the α th phase as a function of the points $X \in \mathcal{C}_R$, we
 181 perform the composition $\mathbf{u}_\alpha(\cdot, t) = \mathbf{v}_\alpha(\cdot, t) \circ \chi(\cdot, t)$. However, from now on
 182 we shall omit the explicit dependence on time in the composition of functions,
 183 so that, for example, the velocity field $\mathbf{u}_\alpha : \mathcal{C}_R \times \mathcal{J} \rightarrow T\mathcal{S}$ shall be simply denoted
 184 by $\mathbf{u}_\alpha = \mathbf{v}_\alpha \circ \chi$.

185 The tangent map of $\chi(\cdot, t)$ at $X \in \mathcal{C}_R$ defines the deformation gradient
 186 tensor of the solid motion, $\mathbf{F}(X, t) = T\chi(X, t) : T_X\mathcal{C}_R \rightarrow T_x\mathcal{S}$. In order for
 187 χ to be admissible, the condition $J = \det(\mathbf{F}) > 0$ must be respected at all
 188 points and all times. The transpose, inverse, and transpose inverse of \mathbf{F} are
 189 defined as $\mathbf{F}^T : T^*\mathcal{S} \rightarrow T^*\mathcal{C}_R$, $\mathbf{F}^{-1} : T\mathcal{S} \rightarrow T\mathcal{C}_R$, and $\mathbf{F}^{-T} : T^*\mathcal{C}_R \rightarrow T^*\mathcal{S}$,
 190 respectively. It also holds that $\mathbf{G}^{-1} \mathbf{F}^T \mathbf{g} : T\mathcal{S} \rightarrow T\mathcal{C}_R$. This combination of
 191 tensors shall be used in the definition of the Mandel stress tensors (cf. Sect. 3).
 192 The symmetric, positive definite, second-order tensor $\mathbf{C} = \mathbf{F}^T \mathbf{g} \mathbf{F} \in [T\mathcal{C}_R]_2^0$
 193 is the Cauchy-Green deformation tensor induced by \mathbf{F} . For $\alpha = s, f$, we also
 194 introduce the spatial velocity gradient $\ell_\alpha = (\text{grad } \mathbf{v}_\alpha) \circ \chi \in T\mathcal{S} \otimes T^*\mathcal{S}$, which
 195 is related to the “material” velocity gradient, $\text{Grad } \mathbf{u}_\alpha \in T\mathcal{S} \otimes T^*\mathcal{C}_R$, through
 196 $\text{Grad } \mathbf{u}_s = \dot{\mathbf{F}} = \ell_s \mathbf{F}$ and $\text{Grad } \mathbf{u}_f := \ell_f \mathbf{F}$, respectively.

197 2.2 The Bilby-Kröner-Lee (BKL) decomposition for porous media

198 In this work, we study the remodelling that occurs in a biological system when,
 199 under appropriate loading conditions, the system is compelled to reorganise its

internal structure in order to sustain the applied loads. In the case of cellular aggregates [42], this type of remodelling manifests itself through the structural transformation of the actin network in the cells, and the reorganisation of the adhesion bonds among the cells. In soft tissues, such as articular cartilage, the considered remodelling might represent the rearrangement of the cross-links of the fibre network forming the extracellular matrix. These processes can be described in terms of “plastic distortions” [42]. It is important to recall that this kind of remodelling is characterised by time scales (in fact, those induced by the mechanical loads) that allow to decouple it from the structural evolution ascribable to growth. Growth, indeed, is due to the mitosis and apoptosis of the cells, which typically occur over sufficiently larger time scales. For this reason, we disregard growth-related aspects of remodelling in the present framework.

To describe the deformation and the plastic distortions that accompany the remodelling of the biological system under study, we introduce, in addition to \mathbf{F} , the “tensor of plastic distortions” \mathbf{F}_p . This leads us to the Bilby-Kröner-Lee (BKL) multiplicative decomposition $\mathbf{F} = \mathbf{F}_e \mathbf{F}_p$, where \mathbf{F}_e is sometimes referred to as the “accommodating part” of the overall deformation gradient tensor. To sketch the conceptual meaning of \mathbf{F}_p , we refer to [71]. Hence, we consider a body that is brought from its reference, unloaded configuration, \mathcal{C}_R , to the current configuration, \mathcal{C}_t , by the action of applied loads. If this evolution is accompanied by a structural reorganisation, the body cannot be brought back to \mathcal{C}_R by removing the external loads. Rather, even though all external loads were removed, the system would occupy a configuration different from \mathcal{C}_t and \mathcal{C}_R , in which residual stresses and residual strains may be present. To eliminate these, one should ideally tear the body to small disjoint pieces (i.e., neighbourhoods of material points), and let each of them individually attain a stress-free state (in doing this ideal tearing, time is kept fixed). The collection of all these stress-free body pieces, determined through the ideal tearing process, is said to be the “natural state” of the body at time t . The plastic distortion \mathbf{F}_p is the distortion that has to be applied to the material neighbourhoods of the points in \mathcal{C}_R to obtain the body pieces collected in the natural state. If the material shows elastic behaviour from its natural state, the accommodating distortion, \mathbf{F}_e , is the elastic distortion that has to be applied to the body elements in the natural state to retrieve the global configuration \mathcal{C}_t . The BKL decomposition can be understood as a combination of “tangent bundle maps” [83], so that one can introduce a time-dependent intermediate map $\chi_\kappa(\cdot, t) : \mathcal{C}_R \rightarrow \mathcal{S}$, which constitutes the base map for \mathbf{F}_p . However, the existence of $\chi_\kappa(\cdot, t)$ does not necessarily imply that \mathbf{F}_p is the tangent map of $\chi_\kappa(\cdot, t)$. In fact, in general, \mathbf{F}_p is neither compatible nor integrable, i.e., there exists no deformation whose tangent map equals \mathbf{F}_p . In the following, we call the set $\chi_\kappa(\mathcal{C}_R, t) = \mathcal{C}_\kappa \subset \mathcal{S}$ “intermediate configuration” (cf. Fig. 2), and associate it with the “natural state” of the solid phase.

Due to the BKL decomposition, the velocity gradient of the solid phase, $\ell_s = \dot{\mathbf{F}} \mathbf{F}^{-1}$, can be written as

$$\ell_s = \ell_e + \ell_p = \ell_e + \mathbf{F}_e \mathbf{L}_p \mathbf{F}_e^{-1}, \quad (3)$$

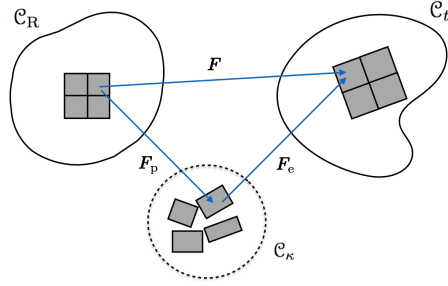


Fig. 2 Schematic representation of the BKL decomposition of the deformation gradient tensor \mathbf{F}

244 where $\ell_e = \dot{\mathbf{F}}_e \mathbf{F}_e^{-1}$ is the rate of elastic distortions, while $\ell_p = \mathbf{F}_e \mathbf{L}_p \mathbf{F}_e^{-1}$
 245 and $\mathbf{L}_p = \dot{\mathbf{F}}_p \mathbf{F}_p^{-1}$ are the rates of anelastic distortions associated with the
 246 current configuration and the natural state of the system, respectively. The
 247 BKL decomposition implies the identity $J = J_e J_p$, where $J_e := \det(\mathbf{F}_e) > 0$
 248 and $J_p := \det(\mathbf{F}_p) > 0$ are referred to as the elastic and anelastic volumetric
 249 ratios, respectively. The rates \dot{J}_e and \dot{J}_p can be computed as $\dot{J}_e = J_e \text{tr}(\ell_e)$ and
 250 $\dot{J}_p = J_p \text{tr}(\mathbf{L}_p) = J_p \text{tr}(\ell_p)$. In the following, we shall assume that the anelastic
 251 distortions related to remodelling are volume-preserving, thereby leading to
 252 the constraint $J_p = \det(\mathbf{F}_p) = 1$, which implies $\text{tr}(\ell_p) = 0$ and $\text{tr}(\mathbf{L}_p) = 0$.

253 For future use, we introduce $\boldsymbol{\eta}$, i.e., the metric tensor associated with the
 254 intermediate configuration \mathcal{C}_k , and $\mathbf{B}_p := \mathbf{C}_p^{-1}$, where $\mathbf{C}_p = \mathbf{F}_p^T \boldsymbol{\eta} \mathbf{F}_p$ is the
 255 anelastic Cauchy-Green deformation tensor. Moreover, we shall exploit the
 256 kinematic identity

$$\frac{1}{2} \dot{\mathbf{B}}_p = -\mathbf{F}_p^{-1} (\boldsymbol{\eta}^{-1} \mathbf{D}_p \boldsymbol{\eta}^{-1}) \mathbf{F}_p^{-T}, \quad (4)$$

257 where $\mathbf{D}_p := \text{sym}(\boldsymbol{\eta} \mathbf{L}_p)$.

258 2.3 Dynamics of biphasic mixtures

259 In the absence of external body forces, growth, and mass exchange processes
 260 between the solid and the fluid phase, the local forms of the mass and linear
 261 momentum balance laws for the α th phase of the biphasic mixture ($\alpha = s, f$)
 262 can be written as

$$\partial_t(\phi_\alpha \varrho_\alpha) + \text{div}(\phi_\alpha \varrho_\alpha \mathbf{v}_\alpha) = 0, \quad \text{in } \mathcal{C}_t \times \mathcal{J}, \quad (5a)$$

$$\phi_\alpha \varrho_\alpha \mathbf{a}_\alpha = \text{div} \boldsymbol{\sigma}_\alpha + \mathbf{m}_\alpha, \quad \text{in } \mathcal{C}_t \times \mathcal{J}, \quad (5b)$$

$$\mathbf{m}_s + \mathbf{m}_f = \mathbf{0}, \quad \text{in } \mathcal{C}_t \times \mathcal{J}. \quad (5c)$$

263 In (5), ϕ_α and ϱ_α denote, respectively, the volumetric fraction and the true
 264 mass density of the α th phase, $\boldsymbol{\sigma}_\alpha$ is the Cauchy stress tensor, and \mathbf{m}_α is
 265 the rate of linear momentum exchange between the α th phase and the other

one. Equation (5c) expresses that the mixture is closed with respect to linear momentum.

If we assume that the pore space of the matrix is completely filled with the fluid, the volumetric fractions ϕ_s and ϕ_f are constrained by the saturation condition $\phi_s + \phi_f = 1$, which has to be respected at all times and at all points of the mixture. In the following, ϱ_s and ϱ_f shall be assumed to be given constants. Moreover, it will be hypothesised that the inertial terms $\phi_\alpha \varrho_\alpha \mathbf{a}_\alpha$ are negligible. This latter hypothesis leads to a quasi-static formulation of the problem, in which the only sources of time evolution for the system are provided by time-varying boundary conditions, a (slowly) time-evolving deformation, and the presence of the time-dependent reorganisation of the tissue's internal structure. By accounting for (5c), and summing (5b) over $\alpha = s, f$, we obtain

$$\operatorname{div}(\boldsymbol{\sigma}_s + \boldsymbol{\sigma}_f) = \mathbf{0}, \quad \text{in } \mathcal{C}_t \times \mathcal{J}, \quad (6a)$$

$$\operatorname{div} \boldsymbol{\sigma}_f + \mathbf{m}_f = \mathbf{0}, \quad \text{in } \mathcal{C}_t \times \mathcal{J}. \quad (6b)$$

Transforming (5a) by the backward Piola-transformation induced by the solid motion $\chi(\cdot, t)$, and writing the transformed equation once for $\alpha = s$ and once for $\alpha = f$, it is possible to show that, after some manipulations, the mass balance laws for the solid and the fluid phase reduce to [44, 45]

$$\phi_s(\chi_s(X, t), t) = \frac{\phi_{sR}(X)}{J(X, t)}, \quad \text{in } \mathcal{C}_R \times \mathcal{J}, \quad (7a)$$

$$\dot{J} + \operatorname{Div} [(J - \phi_{sR}) \mathbf{F}^{-1} \mathbf{u}_{fs}] = 0, \quad \text{in } \mathcal{C}_R \times \mathcal{J}, \quad (7b)$$

with $\mathbf{u}_{fs} = \mathbf{u}_f - \mathbf{u}_s = \mathbf{v}_{fs} \circ \chi$. In (7a), $\phi_{sR}(X)$ represents the volumetric fraction of the solid phase in the reference configuration. Since ϕ_{sR} does not depend on time in the present framework, it can be chosen as a referential value for ϕ_s . We remark that, in the presence of growth, or in the case of non-isochoric plastic distortions, the condition $J_p = 1$ does not necessarily apply, which means that ϕ_{sR} is not time-independent in general. Rather, in the presence of density-preserving growth [62, 63], it can only be inferred that the volumetric fraction associated with the intermediate configuration, i.e., $\phi_{sn}(X) := J_e(X, t) \phi_s(\chi(X, t), t)$, is constant in time.

3 Constitutive framework and remodelling law

If the solid phase exhibits hyperelastic material behaviour from its natural state, and if the fluid phase can be regarded as macroscopically inviscid, then admissible expressions of the Cauchy stresses $\boldsymbol{\sigma}_s$ and $\boldsymbol{\sigma}_f$ are given by

$$\boldsymbol{\sigma}_s = -\phi_s p \mathbf{g}^{-1} + \boldsymbol{\sigma}_{sc}, \quad (8a)$$

$$\boldsymbol{\sigma}_f = -\phi_f p \mathbf{g}^{-1}, \quad (8b)$$

295 where $\boldsymbol{\sigma}_{\text{sc}}$ is the constitutive part of the Cauchy stress associated with the
 296 solid phase, i.e.,

$$\boldsymbol{\sigma}_{\text{sc}} \circ \chi = \frac{1}{J_e} \mathbf{F}_e \left(2 \frac{\partial \hat{W}_{\text{s}\kappa}}{\partial \mathbf{C}_e}(\mathbf{C}_e) \right) \mathbf{F}_e^{\text{T}}. \quad (9)$$

297 In (9), $\hat{W}_{\text{s}\kappa}$ is the strain energy density function of the solid phase, expressed
 298 per unit volume of the intermediate configuration, and $\mathbf{C}_e = \mathbf{F}_p^{-\text{T}} \mathbf{C} \mathbf{F}_p^{-1}$ is
 299 the elastic Cauchy-Green deformation tensor. In this work, we assume that
 300 $\hat{W}_{\text{s}\kappa}$ is of the Holmes-Mow type [57], i.e.,

$$\hat{W}_{\text{s}\kappa}(\mathbf{C}_e) = \alpha_0 \{ \exp(\Psi(\mathbf{C}_e)) - 1 \}, \quad (10a)$$

$$\Psi(\mathbf{C}_e) = \alpha_1 [\hat{I}_1(\mathbf{C}_e) - 3] + \alpha_2 [\hat{I}_2(\mathbf{C}_e) - 3] - \beta \log[\hat{I}_3(\mathbf{C}_e)], \quad (10b)$$

301 where α_0 , α_1 , α_2 , and β are model parameters, while \hat{I}_1 , \hat{I}_2 , and \hat{I}_3 are the
 302 invariants of \mathbf{C}_e , i.e.,

$$I_1 = \hat{I}_1(\mathbf{C}_e) = \text{tr}(\boldsymbol{\eta}^{-1} \mathbf{C}_e) = \text{tr}(\mathbf{B}_p \mathbf{C}), \quad (11a)$$

$$I_2 = \hat{I}_2(\mathbf{C}_e) = \frac{1}{2} \{ [I_1(\mathbf{C}_e)]^2 - \text{tr}[(\boldsymbol{\eta}^{-1} \mathbf{C}_e)^2] \} = \frac{1}{2} \{ I_1^2 - \text{tr}[(\mathbf{B}_p \mathbf{C})^2] \}, \quad (11b)$$

$$I_3 = \hat{I}_3(\mathbf{C}_e) = \det(\mathbf{C}_e) = J_e^2 = J^2, \quad (11c)$$

303 where the last equality in (11c) is due to the hypothesis of isochoric plastic
 304 distortions, i.e., $J_p = 1$. The strain energy density function $\hat{W}_{\text{s}\kappa}$ describes
 305 a material exhibiting isotropic elastic properties with respect to the natural
 306 state. In general, if the model of the considered tissue is inhomogeneous, the
 307 parameters α_0 , α_1 , α_2 , and β depend on material points. Sometimes, however,
 308 for computational simplicity, or because of lack of experimental data, it is as-
 309 sumed that only one of these parameters is variable. For instance, in modelling
 310 articular cartilage [46], α_0 was expressed by fitting experimental data taken
 311 from the literature as a third-order polynomial function of the axial coordinate
 312 parameterising the depth of a cylindrical specimen of tissue, whereas all the
 313 other material parameters were assumed to be constant.

314 The expressions of $\boldsymbol{\sigma}_s$ and $\boldsymbol{\sigma}_f$ reported in (8a) and (8b) can be found in
 315 many works based on Mixture Theory (cf. e.g. [25,81,91]). Here, they have
 316 been adapted from [15,56] to the case of an incompressible, single-constituent
 317 fluid phase, as previously done in [34,35,45,94]. By substituting (8a) and (8b)
 318 into (6a) and (6b), the momentum balance laws for the mixture as a whole
 319 and for the fluid phase become [56]

$$\text{div}(-p \mathbf{g}^{-1} + \boldsymbol{\sigma}_{\text{sc}}) = \mathbf{0}, \quad \text{in } \mathcal{C}_t \times \mathcal{J}, \quad (12a)$$

$$-\mathbf{g}^{-1}(\phi_f \text{grad } p) + (\mathbf{m}_f - p \mathbf{g}^{-1} \text{grad } \phi_f) = \mathbf{0}, \quad \text{in } \mathcal{C}_t \times \mathcal{J}. \quad (12b)$$

320 To determine the material form of the momentum balance law for the mixture
 321 as whole, i.e., the material counterpart of (12a), we introduce the first Piola-
 322 Kirchhoff stress tensors

$$\mathbf{P}_s = J \boldsymbol{\sigma}_s \mathbf{F}^{-\text{T}} = -\phi_{\text{sR}} p \mathbf{g}^{-1} \mathbf{F}^{-\text{T}} + \mathbf{P}_{\text{sc}}, \quad (13a)$$

$$\mathbf{P}_f = J \boldsymbol{\sigma}_f \mathbf{F}^{-\text{T}} = -(J - \phi_{\text{sR}}) p \mathbf{g}^{-1} \mathbf{F}^{-\text{T}}, \quad (13b)$$

323 where $\mathbf{P}_{\text{sc}} = J\boldsymbol{\sigma}_{\text{sc}}\mathbf{F}^{-\text{T}}$ is the constitutive part of \mathbf{P}_{s} , and perform the Piola-
324 transformation of (12a), i.e.,

$$\text{Div} \left(-Jp\mathbf{g}^{-1}\mathbf{F}^{-\text{T}} + \mathbf{P}_{\text{sc}} \right) = \mathbf{0}, \quad \text{in } \mathcal{C}_{\text{R}} \times \mathcal{J}. \quad (14)$$

325 By adopting the strain energy density function \hat{W}_{srk} specified in (10a) and (10b),
326 \mathbf{P}_{sc} can be expressed constitutively as a function of \mathbf{F} and \mathbf{B}_{p} , i.e.,

$$\begin{aligned} \mathbf{P}_{\text{sc}} = \hat{\mathbf{P}}_{\text{sc}}(\mathbf{F}, \mathbf{B}_{\text{p}}) &= 2b_1\mathbf{F}\mathbf{B}_{\text{p}} + 2b_2(I_1\mathbf{F}\mathbf{B}_{\text{p}} - \mathbf{F}\mathbf{B}_{\text{p}}\mathbf{C}\mathbf{B}_{\text{p}}) \\ &+ 2b_3I_3\mathbf{g}^{-1}\mathbf{F}^{-\text{T}}, \end{aligned} \quad (15)$$

327 where $b_i = \hat{b}_i(\mathbf{F}, \mathbf{B}_{\text{p}}) = \frac{\partial \hat{W}_{\text{srk}}}{\partial I_i}(\mathbf{F}, \mathbf{B}_{\text{p}})$, $i = 1, 2, 3$, are constitutive functions of
328 the invariants of \mathbf{C}_{e} , and can be thus written as functions of \mathbf{F} and \mathbf{B}_{p} . Hence,
329 the overall stress $\mathbf{P} := \mathbf{P}_{\text{s}} + \mathbf{P}_{\text{f}}$, which has to be substituted into (14), reads

$$\mathbf{P} = \hat{\mathbf{P}}(p, \mathbf{F}, \mathbf{B}_{\text{p}}) = -Jp\mathbf{g}^{-1}\mathbf{F}^{-\text{T}} + \hat{\mathbf{P}}_{\text{sc}}(\mathbf{F}, \mathbf{B}_{\text{p}}). \quad (16)$$

330 For future use, we also introduce the Kirchhoff stress tensor $\boldsymbol{\tau} = \mathbf{P}\mathbf{F}^{\text{T}}$ and
331 the Mandel stress tensor $\boldsymbol{\Sigma} = \mathbf{G}^{-1}\mathbf{F}^{\text{T}}\mathbf{g}\boldsymbol{\tau}\mathbf{F}^{-\text{T}}$, i.e.,

$$\boldsymbol{\tau} = \hat{\boldsymbol{\tau}}(p, \mathbf{F}, \mathbf{B}_{\text{p}}) = -Jp\mathbf{g}^{-1} + \hat{\boldsymbol{\tau}}_{\text{sc}}(\mathbf{F}, \mathbf{B}_{\text{p}}), \quad (17a)$$

$$\boldsymbol{\Sigma} = \hat{\boldsymbol{\Sigma}}(p, \mathbf{F}, \mathbf{B}_{\text{p}}) = -Jp\mathbf{G}^{-1} + \hat{\boldsymbol{\Sigma}}_{\text{sc}}(\mathbf{F}, \mathbf{B}_{\text{p}}). \quad (17b)$$

332 In (17a) and (17b), the constitutive parts of $\boldsymbol{\tau}$ and $\boldsymbol{\Sigma}$, given by $\boldsymbol{\tau}_{\text{sc}} = \hat{\boldsymbol{\tau}}_{\text{sc}}(\mathbf{F}, \mathbf{B}_{\text{p}})$
333 and $\boldsymbol{\Sigma}_{\text{sc}} = \hat{\boldsymbol{\Sigma}}_{\text{sc}}(\mathbf{F}, \mathbf{B}_{\text{p}})$, respectively, read

$$\begin{aligned} \boldsymbol{\tau}_{\text{sc}} = \hat{\boldsymbol{\tau}}_{\text{sc}}(\mathbf{F}, \mathbf{B}_{\text{p}}) &= (2b_1 + 2b_2I_1)\mathbf{F}\mathbf{B}_{\text{p}}\mathbf{F}^{\text{T}} - 2b_2\mathbf{F}\mathbf{B}_{\text{p}}\mathbf{C}\mathbf{B}_{\text{p}}\mathbf{F}^{\text{T}} \\ &+ 2b_3I_3\mathbf{g}^{-1}, \end{aligned} \quad (18a)$$

$$\begin{aligned} \boldsymbol{\Sigma}_{\text{sc}} = \hat{\boldsymbol{\Sigma}}_{\text{sc}}(\mathbf{F}, \mathbf{B}_{\text{p}}) &= (2b_1 + 2b_2I_1)\mathbf{G}^{-1}\mathbf{C}\mathbf{B}_{\text{p}} - 2b_2\mathbf{G}^{-1}\mathbf{C}\mathbf{B}_{\text{p}}\mathbf{C}\mathbf{B}_{\text{p}} \\ &+ 2b_3I_3\mathbf{G}^{-1}. \end{aligned} \quad (18b)$$

334 We remark that, although $\boldsymbol{\Sigma}_{\text{sc}}$ is not symmetric in general, the assumption of
335 isotropic hyperelastic response of the solid phase, which leads to (18b), implies
336 the symmetry conditions [69]

$$\mathbf{B}_{\text{p}}\mathbf{G}\boldsymbol{\Sigma}_{\text{sc}} = (\mathbf{B}_{\text{p}}\mathbf{G}\boldsymbol{\Sigma}_{\text{sc}})^{\text{T}}, \quad (19a)$$

$$\mathbf{G}\boldsymbol{\Sigma}_{\text{sc}}\mathbf{B}_{\text{p}}^{-1} = (\mathbf{G}\boldsymbol{\Sigma}_{\text{sc}}\mathbf{B}_{\text{p}}^{-1})^{\text{T}}. \quad (19b)$$

337 3.1 Dissipation inequality

338 The local form of the dissipation inequality characterising the biphasic system
339 under investigation can be written as follows

$$D_{\text{m}} = -\{\mathbf{m}_{\text{f}} - p\mathbf{g}^{-1}\text{grad } \phi_{\text{f}}\} \cdot \mathbf{v}_{\text{fs}} + \boldsymbol{\sigma}_{\text{sc}} : \mathbf{g}\boldsymbol{\ell}_{\text{p}} \geq 0, \quad (20)$$

where D_m is the dissipation function of the mixture as a whole, written per unit volume of \mathcal{C}_t (cf. [15, 44, 56] for details). Note that, more rigorously, and for consistency with (3), we should write $\sigma_{sc} : \mathbf{g}(\ell_p \circ \chi^{-1})$ in (20). However, for the sake of a lighter notation, we shall omit the composition of maps in the forthcoming calculations. Since ℓ_p has vanishing trace, only the deviatoric part of σ_{sc} contributes to the dissipation D_m . Following [15, 56, 94], \mathbf{m}_f can be written as

$$\mathbf{m}_f = \mathbf{m}_{fd} + p \mathbf{g}^{-1} \text{grad } \phi_f, \quad (21)$$

where \mathbf{m}_{fd} and $p \mathbf{g}^{-1} \text{grad } \phi_f$ represent, respectively, the dissipative and the non-dissipative contribution to \mathbf{m}_f . By substituting (21) into (12b), we obtain

$$\mathbf{m}_{fd} = \mathbf{g}^{-1} (\phi_f \text{grad } p). \quad (22)$$

Moreover, the dissipation inequality (20) takes on the form

$$D_m = D_{\text{flow}} + D_{\text{rem}} = \underbrace{-\mathbf{m}_{fd} \cdot \mathbf{v}_{fs}}_{D_{\text{flow}}} + \underbrace{\sigma_{sc} : \mathbf{g} \ell_p}_{D_{\text{rem}}} \geq 0. \quad (23)$$

The inequality (23) states that, within a purely mechanical framework, the only two sources of dissipation for the considered biphasic system are given by $D_{\text{flow}} := -\mathbf{m}_{fd} \cdot \mathbf{v}_{fs}$, i.e., the power expended by the dissipative force \mathbf{m}_{fd} , which is power-conjugate with the relative velocity \mathbf{v}_{fs} , and by $D_{\text{rem}} := \sigma_{sc} : \mathbf{g} \ell_p$, i.e., the power expended to trigger the evolution of the internal structure of the solid phase.

3.1.1 Darcy's law

We assume that the dissipative force \mathbf{m}_{fd} can be expressed constitutively as a linear function of the filtration velocity $\mathbf{q} := \phi_f \mathbf{v}_{fs}$ [14], i.e.,

$$\mathbf{m}_{fd} = -\mathbf{g}^{-1} \mathbf{r} \phi_f \mathbf{v}_{fs}, \quad (24)$$

where $\mathbf{r} \in [TS]_2^0$ is the tensor describing the resistivity of the porous medium to fluid flow [56]. By substituting (24) into (23), the following expression of dissipation is obtained

$$D_m = D_{\text{flow}} + D_{\text{rem}} = \underbrace{\text{sym}(\mathbf{r}) : \phi_f (\mathbf{v}_{fs} \otimes \mathbf{v}_{fs})}_{D_{\text{flow}}} + \underbrace{\sigma_{sc} : \mathbf{g} \ell_p}_{D_{\text{rem}}} \geq 0, \quad (25)$$

where $\text{sym}(\mathbf{r})$ is the symmetric part of \mathbf{r} . A direct consequence of (25) is that, if $\text{sym}(\mathbf{r})$ is positive semi-definite, D_{flow} is always non-negative, i.e., $D_{\text{flow}} \geq 0$, for any possible realisation of the relative velocity \mathbf{v}_{fs} . Typically, the resistivity tensor \mathbf{r} is assumed to be symmetric and positive definite, so that \mathbf{m}_{fd} vanishes if, and only if, \mathbf{v}_{fs} is null. Under these assumptions, and the further hypothesis that \mathbf{m}_{fd} is linear in \mathbf{v}_{fs} , the standard form of Darcy's law is obtained. Indeed, by substituting (24) into (22), and solving for $\phi_f \mathbf{v}_{fs}$, the filtration velocity is found to be

$$\mathbf{q} = \phi_f \mathbf{v}_{fs} = -\mathbf{k} \text{grad } p, \quad (26)$$

370 where $\mathbf{k} = \phi_f \mathbf{r}^{-1} \in [TS]_0^2$ is the hydraulic conductivity tensor of the system.

371 By performing a Piola transformation of (26), we obtain the material form
372 of Darcy's law:

$$J\mathbf{F}^{-1}(\phi_f \mathbf{u}_{fs}) = (J - \phi_{sR})\mathbf{F}^{-1}\mathbf{u}_{fs} = -\mathbf{K}\text{Grad } p. \quad (27)$$

373 The material second-order tensor $\mathbf{K} = J\mathbf{F}^{-1}\mathbf{k}\mathbf{F}^{-T}$ is the material hydraulic
374 conductivity tensor, and is determined by means of the Piola transformation
375 of \mathbf{k} with respect to the solid motion. Substituting (27) into (7b) yields

$$\dot{J} - \text{Div}[\mathbf{K}\text{Grad } p] = 0. \quad (28)$$

376 The constitutive law defining the hydraulic conductivity, \mathbf{k} , should comply
377 with the material symmetries of the considered tissue (e.g., isotropy, trans-
378 verse isotropy, or orthotropy). Recently, a review on several constitutive laws
379 expressing \mathbf{k} as a function of the tissue deformation has been given in [13]. An
380 expression of \mathbf{k} suitable for articular cartilage was determined by employing
381 upscaling arguments in the small deformation regime [36, 37], and subsequently
382 adapted to the finite-deformation framework in [34, 35, 94]. If the hydraulic re-
383 sponse of the mixture is isotropic, and the hypothesis is made that the isotropy
384 of the hydraulic conductivity does not change with the deformation, the ten-
385 sors \mathbf{k} and \mathbf{K} can be expressed constitutively as

$$\mathbf{k} = \hat{\mathbf{k}}(J) = \hat{k}_0(J)\mathbf{g}^{-1}, \quad (29a)$$

$$\mathbf{K} = \hat{\mathbf{K}}(\mathbf{F}) = J\hat{k}_0(J)\mathbf{C}^{-1}, \quad (29b)$$

386 where the scalar hydraulic conductivity function \hat{k}_0 is given by

$$\hat{k}_0(J) = k_{0R} \left(\frac{J - \phi_{sR}}{1 - \phi_{sR}} \right)^{m_0} \exp \left[\frac{m_1}{2}(J^2 - 1) \right], \quad (30)$$

387 and m_0 and m_1 are material parameters [57]. According to (29a) and (30),
388 the deformation influences the hydraulic conductivity through the volumetric
389 ratio J only. When the condition $J = 1$ is met, the identity $\hat{k}_0(1) = k_{0R}$ is
390 obtained, which means that the scalar hydraulic conductivity becomes equal
391 to the referential one, k_{0R} . In general, k_{0R} , m_0 , and m_1 depend on material
392 points. The constitutive choice of the hydraulic conductivity tensor permits to
393 express D_{flow} constitutively as

$$D_{\text{flow}} = \hat{D}_{\text{flow}}(J, \text{grad } p) = \hat{\mathbf{k}}(J) : \text{grad } p \otimes \text{grad } p \geq 0, \quad (31)$$

394 with \hat{D}_{flow} being quadratic in $\text{grad } p$, and highly non-linear in J .

3.1.2 Law of remodelling

In this section, we introduce the fundamental hypotheses that lead to the law of remodelling adopted in our work. We recall that, as announced in Sect. 2.2, we are considering a type of structural evolution that can be interpreted in terms of isochoric plastic distortions. Therefore, the first hypothesis is that \mathbf{F}_p is restricted by the constraint $J_p = \det(\mathbf{F}_p) = 1$. This implies that the rates of plastic distortions, ℓ_p or \mathbf{L}_p , are deviatoric, i.e., $\text{tr}(\ell_p) = 0$, and $\text{tr}(\mathbf{L}_p) = 0$. A direct consequence of these facts is that the part of the dissipation function related to remodelling, i.e., D_{rem} , can be written as

$$D_{\text{rem}} = \sigma_{\text{sc}} : \mathbf{g}\ell_p = J_e^{-1} \boldsymbol{\Sigma}_{\text{sc}\kappa} : \boldsymbol{\eta}\mathbf{L}_p \geq 0. \quad (32)$$

The tensor $\boldsymbol{\Sigma}_{\text{sc}\kappa} := J_e \boldsymbol{\eta}^{-1} \mathbf{F}_e^{\text{T}} \mathbf{g} \sigma_{\text{sc}} \mathbf{F}_e^{-\text{T}}$ is the constitutive part of the solid phase Mandel stress tensor as computed with respect to the natural state, and represents the measure of stress power-conjugate to \mathbf{L}_p . The prescription on the non-negativeness of D_{rem} is due to the Principle of Maximum Dissipation (cf. e.g. [53]), which is based on the requirement that the overall dissipation function, D_m , be non-negative for all possible realisations of the generalised velocities $\phi_f \mathbf{v}_{\text{fs}}$ and ℓ_p (or \mathbf{L}_p). Thus, in the case in which the fluid filtration velocity is null, which implies $D_{\text{flow}} = 0$, it must hold that $D_m = D_{\text{rem}} \geq 0$. We remark that the expression of D_{rem} given in (32) appears quite naturally in all the theories of anelastic processes constructed on the BKL decomposition (cf. e.g. [22, 65, 69] for the case of finite strain Elastoplasticity, and [31, 40, 42, 45, 48, 49, 61, 64] for the case of growth and remodelling of biological tissues), and stems from the hypothesis that the strain energy density of the solid phase, \hat{W}_{sc} , can be written as a constitutive function of the elastic part of the overall deformation alone, \mathbf{C}_e , as done in (9). By relating \mathbf{F}_p with the production of material inhomogeneities in uniform bodies [31], a rationale for this constitutive hypothesis is obtained by invoking the Principle of Material Uniformity [29–31, 83].

The second hypothesis is that the solid phase exhibits isotropic elastic behaviour from its natural state. Since this property implies the symmetry of $\boldsymbol{\Sigma}_{\text{sc}\kappa}$, D_{rem} can be rewritten as $D_{\text{rem}} = J_e^{-1} \boldsymbol{\Sigma}_{\text{sc}\kappa} : \mathbf{D}_p$. Hence, by exploiting the kinematic identity (4), recalling the relation $J_p \boldsymbol{\Sigma}_{\text{sc}\kappa} = \boldsymbol{\eta}^{-1} \mathbf{F}_p^{-\text{T}} \mathbf{G} \boldsymbol{\Sigma}_{\text{sc}} \mathbf{F}_p^{\text{T}}$ that links $\boldsymbol{\Sigma}_{\text{sc}\kappa}$ with $\boldsymbol{\Sigma}_{\text{sc}}$, and accounting for the symmetry condition (19b), it is possible to show that D_{rem} admits the equivalent form

$$D_{\text{rem}} = -\frac{1}{2J} (\mathbf{G} \boldsymbol{\Sigma}_{\text{sc}} \mathbf{B}_p^{-1}) : \dot{\mathbf{B}}_p. \quad (33)$$

Moreover, since the condition $J_p = 1$ can be rephrased as $\mathbf{B}_p^{-1} : \dot{\mathbf{B}}_p = 0$, only the deviatoric part of $\boldsymbol{\Sigma}_{\text{sc}}$ contributes to D_{rem} . Consequently, D_{rem} becomes

$$D_{\text{rem}} = -\frac{1}{2J} [\mathbf{G} \text{dev}(\boldsymbol{\Sigma}_{\text{sc}}) \mathbf{B}_p^{-1}] : \dot{\mathbf{B}}_p \geq 0, \quad (34)$$

with

$$\text{dev}(\boldsymbol{\Sigma}_{\text{sc}}) = \boldsymbol{\Sigma}_{\text{sc}} - \frac{1}{3} \text{tr}[\mathbf{G} \boldsymbol{\Sigma}_{\text{sc}}] \mathbf{G}^{-1}. \quad (35)$$

431 Note that a direct consequence of the hypothesis of isotropy is that the plastic
 432 flow rule can be expressed in terms of \mathbf{B}_p , rather than \mathbf{F}_p . If, on the one hand,
 433 this leads to a loss of information, on the other hand, computations become
 434 much lighter.

435 The third hypothesis concerns the type of remodelling addressed in this
 436 paper. As anticipated in Sect. 2.2, we assume that the considered system re-
 437 models when the stress induced by external loading exceeds a characteristic
 438 threshold, thereby triggering the onset of plastic distortions. Hence, as we
 439 would do in the theory of Elastoplasticity, we search for an evolution law for
 440 the remodelling variable \mathbf{B}_p in the form of a generalised plastic “flow rule”. To
 441 this end, following [42], we imitate the theory of associative, rate-independent
 442 Elastoplasticity [22,93], and articulate in two steps the determination of the
 443 flow rule. In the first step, we postulate that a yield surface exists in the space
 444 of the deviatoric Kirchhoff stress tensors, which can be defined by the equation

$$f(\boldsymbol{\tau}_{sc}) := \varphi(\boldsymbol{\tau}_{sc}) - \sqrt{(2/3)}\tau_y = 0. \quad (36)$$

445 Here, $\tau_y > 0$ is a scalar measure of stress playing the role of the “yield stress”
 446 of the considered material, and $\varphi(\boldsymbol{\tau}_{sc})$ is given by

$$\varphi(\boldsymbol{\tau}_{sc}) := \|\text{dev}(\boldsymbol{\tau}_{sc})\| = \sqrt{\text{tr}[(\mathbf{g}\text{dev}(\boldsymbol{\tau}_{sc}))^2]}. \quad (37)$$

447 In the second step, we require that the plastic flow is orthogonal to the yield
 448 surface. This leads to the “normality rule” [92,93]

$$\mathcal{L}_{\mathbf{v}_s} \mathbf{b}_e = -2\gamma_p \mathbf{n} \mathbf{g} \mathbf{b}_e, \quad (38)$$

449 where $\mathcal{L}_{\mathbf{v}_s} \mathbf{b}_e$ is the Lie derivative of $\mathbf{b}_e = \mathbf{F}_e \boldsymbol{\eta}^{-1} \mathbf{F}_e^T = \mathbf{F} \mathbf{B}_p \mathbf{F}^T$ (i.e., the
 450 elastic left Cauchy deformation tensor) with respect to the velocity of the solid
 451 phase, \mathbf{v}_s , $\gamma_p \geq 0$ is a non-negative function of stress, and \mathbf{n} is the normalised
 452 Kirchhoff stress tensor, orthogonal to the yield surface, defined by

$$\mathbf{n}^b := \mathbf{g} \mathbf{n} \mathbf{g} = \frac{\partial f}{\partial \boldsymbol{\tau}_{sc}}(\boldsymbol{\tau}_{sc}), \quad \mathbf{n} := \frac{\text{dev}(\boldsymbol{\tau}_{sc})}{\|\text{dev}(\boldsymbol{\tau}_{sc})\|}. \quad (39)$$

453 Finally, by exploiting the identity $\mathcal{L}_{\mathbf{v}_s} \mathbf{b}_e = \mathbf{F} \dot{\mathbf{B}}_p \mathbf{F}^T$, and rewriting (38) as an
 454 evolution law for \mathbf{B}_p , we obtain the equivalent flow rule

$$\dot{\mathbf{B}}_p = -2\gamma_p \frac{\mathbf{B}_p \mathbf{G} \text{dev}(\boldsymbol{\Sigma}_{sc})}{\|\text{dev}(\boldsymbol{\tau}_{sc})\|}, \quad (40)$$

455 where, coherently with [42], we set

$$\gamma_p := \lambda \left[\|\text{dev}(\boldsymbol{\tau}_{sc})\| - \sqrt{(2/3)}\tau_y \right]_+ = \lambda [f(\boldsymbol{\tau}_{sc})]_+. \quad (41)$$

456 In (38), (40), and (41), γ_p is a non-negative “plastic” multiplier, λ is a strictly
 457 positive model parameter, and the operator $[\cdot]_+$ is such that, for any real
 458 number A , $[A]_+ = A$, if $A > 0$, and $[A]_+ = 0$ otherwise. The physical units

of γ_p and λ are $[\gamma_p] = \text{s}^{-1}$ and $[\lambda] = (\text{s} \cdot \text{MPa})^{-1}$, respectively. Equation (40), which represents a stress-driven evolution law for the plastic variable \mathbf{B}_p , is the remodelling law sought for. We remark that it complies with the prescription $D_{\text{rem}} \geq 0$. Indeed, by substituting (40) into (34), we obtain

$$D_{\text{rem}} = \hat{D}_{\text{rem}}(\mathbf{F}, \mathbf{B}_p) = \frac{\gamma_p}{J} \|\text{dev}(\boldsymbol{\tau}_{\text{sc}})\| \geq 0. \quad (42)$$

If, for a given choice of the model parameters, \mathbf{F} and \mathbf{B}_p are such that the condition $f(\boldsymbol{\tau}_{\text{sc}}) \leq 0$ applies (which amounts to say that the Frobenius norm of $\boldsymbol{\tau}_{\text{sc}}$ is such that $\|\text{dev}(\boldsymbol{\tau}_{\text{sc}})\| \leq \sqrt{(2/3)}\tau_y$), then it holds that $[f(\boldsymbol{\tau}_{\text{sc}})]_+ = 0$ and, consequently, the plastic multiplier γ_p vanishes identically, thereby implying that $D_{\text{rem}} = 0$. In this situation, no remodelling occurs, and the material deforms while preserving its internal structure. However, when $\|\text{dev}(\boldsymbol{\tau}_{\text{sc}})\|$ exceeds the threshold stress $\sqrt{(2/3)}\tau_y$ (i.e., when $f(\boldsymbol{\tau}_{\text{sc}}) > 0$), remodelling takes place, and \mathbf{B}_p evolves as prescribed by (40). In this case, D_{rem} becomes

$$D_{\text{rem}} = \frac{\lambda[f(\boldsymbol{\tau}_{\text{sc}})]_+}{J} \|\text{dev}(\boldsymbol{\tau}_{\text{sc}})\| > 0. \quad (43)$$

A relevant difference between the model presented so far and the standard model of associative, rate-independent J_2 -plasticity is that γ_p does not stem from any optimality condition of the Karush-Kuhn-Tucker type [22, 93]. Rather, γ_p is defined phenomenologically, and, in the biological context analysed in [42], it expresses the fact that a cellular aggregate, in which the stress exceeds a prescribed threshold value, reorganises its internal structure by breaking the adhesion bonds connecting the cells. Note also that no hardening is considered in this biological problem.

3.2 Summary of the mathematical model

The mathematical model presented in this paper is grounded on the mass balance law (28), the balance law of linear momentum (14), and on the flow rule (40). Thus, in summary, we have to solve the following set of equations:

$$\dot{J} - \text{Div} \left[\hat{\mathbf{K}}(\mathbf{F}) \text{Grad} p \right] = 0, \quad (44a)$$

$$\text{Div} \left(-Jp \mathbf{g}^{-1} \mathbf{F}^{-T} + \hat{\mathbf{P}}_{\text{sc}}(\mathbf{F}, \mathbf{B}_p) \right) = \mathbf{0}, \quad (44b)$$

$$\dot{\mathbf{B}}_p + \hat{\mathbf{R}}(\mathbf{F}, \mathbf{B}_p) = \mathbf{0}, \quad (44c)$$

in which $\hat{\mathbf{K}}(\mathbf{F})$ and $\hat{\mathbf{P}}_{\text{sc}}(\mathbf{F}, \mathbf{B}_p)$ are defined in (29b) and (15), respectively, $\hat{\mathbf{R}}(\mathbf{F}, \mathbf{B}_p)$ stands for

$$\mathbf{R} \equiv \hat{\mathbf{R}}(\mathbf{F}, \mathbf{B}_p) := 2\gamma_p \frac{\mathbf{B}_p \mathbf{G} \text{dev}(\boldsymbol{\Sigma}_{\text{sc}})}{\|\text{dev}(\boldsymbol{\tau}_{\text{sc}})\|}, \quad (45)$$

and γ_p is specified in (41). The model equations (44a)–(44c) are equivalent to a set of ten scalar equations in the ten unknowns represented by the three

487 components of the solid phase motion, χ , pressure, p , and the six indepen-
 488 dent components of the symmetric second-order tensor \mathbf{B}_p . The model is thus
 489 closed. Moreover, it is completed by the following boundary conditions:

$$\chi = \chi_b, \quad \text{on } \Gamma_D^X, \quad (46a)$$

$$\left(-Jp\mathbf{g}^{-1}\mathbf{F}^{-T} + \hat{\mathbf{P}}_{sc}(\mathbf{F}, \mathbf{B}_p)\right) \cdot \mathbf{N} = \mathbf{f}_R, \quad \text{on } \Gamma_N^X, \quad (46b)$$

$$p = p_b, \quad \text{on } \Gamma_D^p, \quad (46c)$$

$$\left(-\hat{\mathbf{K}}(\mathbf{F})\text{Grad}p\right) \cdot \mathbf{N} = Q_b, \quad \text{on } \Gamma_N^p. \quad (46d)$$

490 In (46), \mathbf{N} is the unit vector normal to $\partial\mathcal{C}_R$, i.e., the boundary of the reference
 491 configuration \mathcal{C}_R , and the sets Γ_D^X and Γ_D^p are the Dirichlet-portions of $\partial\mathcal{C}_R$, on
 492 which the deformation, χ , and the pressure, p , are equal to the prescribed data
 493 χ_b and p_b , respectively. Analogously, Γ_N^X and Γ_N^p are the Neumann-portions
 494 of $\partial\mathcal{C}_R$, on which the contact force, \mathbf{f}_R , and the fluid flux, Q_b , are supplied,
 495 respectively. It holds that $\partial\mathcal{C}_R = \Gamma_D^X \sqcup \Gamma_N^X = \Gamma_D^p \sqcup \Gamma_N^p$. The values assigned to
 496 χ_b , p_b , \mathbf{f}_R , and Q_b are problem-dependent and should be discussed on a case-
 497 by-case basis. In the following, however, we shall restrict our formulation to
 498 a problem obeying Neumann-zero boundary conditions on Γ_N^X and Γ_N^p , which
 499 implies $Q_b = 0$ and $\mathbf{f}_R = \mathbf{0}$. Finally, initial conditions are needed because (44a)
 500 and (44c) feature the time derivatives of the volumetric ratio, J , and of the
 501 anelastic deformation tensor \mathbf{B}_p , respectively. Here, we assume the following
 502 initial conditions:

$$J(X, t_0) = 1, \quad \forall X \in \mathcal{C}_R, \quad (47a)$$

$$\mathbf{B}_p(X, t_0) = \mathbf{G}^{-1}, \quad \forall X \in \mathcal{C}_R. \quad (47b)$$

503 For the sake of simplicity, we assume now that the tissue is homogeneous.
 504 Thus, all the elements of the sets of parameters $\{\alpha_0, \alpha_1, \alpha_2, \beta\}$ and $\{m_0, m_1\}$,
 505 which characterise, respectively, the strain energy density function, $\hat{W}_{s\kappa}$, and
 506 the hydraulic conductivity, \mathbf{k} , are regarded as constants. We assume that also
 507 ϕ_{sR} and k_{0R} are constants. Clearly, the hypotheses of homogeneity and isotropy
 508 provide a poor approximation of real tissues. Nonetheless, they are useful
 509 hypotheses at this stage, since they help to better visualise the influence of
 510 remodelling on the mechanical and fluid dynamic properties of the specimen.

511 4 Numerics

512 The numerical procedure elaborated in this paper to solve (44a)–(44c) is based
 513 on the Finite Element Method. Therefore, it is necessary to start with the weak
 514 formulation of (44a) and (44b). Although there exist numerical strategies that
 515 perform finite element discretisations also for the plastic flow rule [32], we
 516 prefer here to keep (44c) in local form. This is legitimate since it involves
 517 no partial derivative with respect to space coordinates. Before proceeding,
 518 we notice that the particular choice of the constitutive law expressing the

519 hydraulic conductivity, $\mathbf{K} = \hat{\mathbf{K}}(\mathbf{F})$, is such that the mass balance law (44a)
 520 does not contain \mathbf{B}_p . This weakens the coupling among the model equations,
 521 as will be discussed in Sect. 6. Our procedure, however, can be generalised to
 522 the cases in which constitutive laws of the type $\mathbf{K} = \hat{\mathbf{K}}(\mathbf{F}, \mathbf{B}_p)$ are employed.

523 4.1 Weak Formulation

524 The weak form of (44a) and (44b) is given by

$$\mathfrak{F}_p(p, \chi, \tilde{p}) := - \int_{\mathcal{C}_R} \left\{ (\text{Grad } \tilde{p}) \left[\hat{\mathbf{K}}(\mathbf{F}) \text{Grad } p \right] + \tilde{p} j \right\} = 0, \quad (48a)$$

$$\mathfrak{F}_\chi(p, \chi, \mathbf{B}_p, \tilde{\mathbf{u}}) := \int_{\mathcal{C}_R} \hat{\mathbf{P}}(p, \mathbf{F}, \mathbf{B}_p) : \mathbf{g} \text{Grad } \tilde{\mathbf{u}} = 0, \quad (48b)$$

525 where $\hat{\mathbf{P}}(p, \mathbf{F}, \mathbf{B}_p)$ is defined in (16), and we introduced the space of test
 526 functions

$$\tilde{\mathcal{P}} \times \tilde{\mathcal{V}} := \{(\tilde{p}, \tilde{\mathbf{u}}) \in H_0^1(\mathcal{C}_R) \times \mathbf{H}_0^1(\mathcal{C}_R) : \tilde{p}|_{\Gamma_D^p} = 0, \tilde{\mathbf{u}}|_{\Gamma_D^x} = \mathbf{0}\}. \quad (49)$$

527 In (48) and (49), \tilde{p} and $\tilde{\mathbf{u}}$ denote the test pressure and the test velocity. As such,
 528 both fields satisfy homogeneous Dirichlet boundary conditions. The functional
 529 spaces $H_0^1(\mathcal{C}_R)$ and $\mathbf{H}_0^1(\mathcal{C}_R)$ are, respectively, the Sobolev spaces of all scalar-
 530 valued and vector-valued functions vanishing on Γ_D^p and Γ_D^x , square-integrable
 531 in \mathcal{C}_R , and whose weak derivatives of order $m \leq 1$ are all square-integrable in
 532 \mathcal{C}_R too. We recall that (48a) and (48b) are obtained by multiplying (44a) by
 533 \tilde{p} and (44b) by $\tilde{\mathbf{u}}$, and applying Gauss' Theorem [59]. By construction, the
 534 functionals \mathfrak{F}_p and \mathfrak{F}_χ are linear in \tilde{p} and $\tilde{\mathbf{u}}$, respectively. For the sake of a
 535 lighter notation, we omit the explicit dependence of \mathfrak{F}_p and \mathfrak{F}_χ on the test
 536 fields \tilde{p} and $\tilde{\mathbf{u}}$ in the forthcoming discussion. This dependence is, however,
 537 understood. Finally, we notice that the use of Darcy's law to describe the fluid
 538 flow implies that both \mathfrak{F}_p and \mathfrak{F}_χ are affine with respect to the pressure p .

539 4.2 Time-discrete setting

540 The time-discrete version of (48a), (48b) and (44c) is obtained by performing
 541 an implicit Euler finite difference scheme. To this end, we discretise the time
 542 interval \mathcal{J} , over which the system is observed, into N disjoint subintervals
 543 $[t_{n-1}, t_n]$, with $n \geq 1$, $n \in \mathbb{N}$, and replace the derivatives \dot{J} and $\dot{\mathbf{B}}_p$ with the
 544 expressions $(J_n - J_{n-1})/\Delta t_n$ and $(\mathbf{B}_{pn} - \mathbf{B}_{p(n-1)})/\Delta t_n$, where Δt_n is the size
 545 of the n th time-step. From here on, given an arbitrary function f of space and
 546 time, the notation $f_n(X)$, or simply f_n , stands for $f(X, t_n)$, for all values of
 547 n .

548 The initial instant of time t_0 corresponds to the reference, undeformed
 549 configuration, \mathcal{C}_R , in which $J_0 = J(X, t_0) = 1$. We also set $\mathbf{B}_{p0} = \mathbf{B}_p(X, t_0) =$
 550 \mathbf{G}^{-1} , thereby implying that no plastic distortion is associated with the initial

551 state of the solid phase. At the n th instant of time, $n \geq 1$, the time-discrete
 552 model equations become:

$$\mathfrak{F}_p(p_n, \chi_n) := - \int_{\mathcal{C}_R} \left\{ (\text{Grad } \tilde{p}) [\mathbf{K}_n \text{Grad } p_n] + \tilde{p} \frac{J_n - J_{n-1}}{\Delta t_n} \right\} = 0, \quad (50a)$$

$$\mathfrak{F}_\chi(p_n, \chi_n, \mathbf{B}_{pn}) := \int_{\mathcal{C}_R} \hat{\mathbf{P}}(p_n, \mathbf{F}_n, \mathbf{B}_{pn}) : \mathbf{g} \text{Grad } \tilde{\mathbf{u}} = 0, \quad (50b)$$

$$\mathfrak{G}(\chi_n, \mathbf{B}_{pn}) := \mathbf{B}_{pn} - \mathbf{B}_{p(n-1)} + \Delta t_n \hat{\mathbf{R}}(\mathbf{F}_n, \mathbf{B}_{pn}) = \mathbf{0}. \quad (50c)$$

553 The notation $\mathfrak{G}(\chi_n, \mathbf{B}_{pn})$ means that the time-discrete form of the plastic
 554 flow rule is a function of \mathbf{B}_{pn} , and a “functional” of the deformation, χ_n ,
 555 through the deformation gradient tensor, \mathbf{F}_n [19]. Equations (50a)–(50c) are
 556 now solved sequentially for varying $n \geq 1$. Apart from (50c), the formulation
 557 of (50a) and (50b) largely follows the procedure presented in [44].

558 4.3 Linearisation and Finite Element Discretisation

559 In this section, we demonstrate in detail the computational procedure, adapted
 560 from [47], that is used to solve numerically (50a)–(50c). We search for solutions
 561 to the problem (50a)–(50c) by means of a linearisation algorithm based on the
 562 Newton method, and articulated in two stages. In addition to n , we introduce
 563 two other subscripts: For each n , $l \in \mathbb{N}$ and $k \in \mathbb{N}$ count the iterations with
 564 respect to \mathbf{B}_{pn} and the pair (p_n, χ_n) , respectively. Consequently, we construct
 565 the sequences

$$\chi_{n,k} = \chi_{n,k-1} + \mathbf{h}_{n,k}, \quad (51a)$$

$$p_{n,k} = p_{n,k-1} + \pi_{n,k}, \quad (51b)$$

$$\mathbf{B}_{pn,l} = \mathbf{B}_{pn,l-1} + \mathfrak{F}_{pn,l}, \quad k, l \geq 1 \quad (51c)$$

566 with $\mathbf{h}_{n,k}$, $\pi_{n,k}$, and $\mathfrak{F}_{pn,l}$ being the increments associated with χ_n , p_n , and
 567 \mathbf{B}_{pn} , respectively. Moreover, for conciseness, we adopt the notation

$$w_n := (p_n, \chi_n), \quad (52a)$$

$$\Theta_{n,l-1} := (\chi_n, \mathbf{B}_{pn,l-1}), \quad (52b)$$

$$A_{n,l-1} := (p_n, \chi_n, \mathbf{B}_{pn,l-1}). \quad (52c)$$

568 In the first stage of the algorithm, we linearise (50b) and (50c) with respect to
 569 \mathbf{B}_{pn} only. The linearisation is done in a neighbourhood of $A_{n,l-1}$ and $\Theta_{n,l-1}$,
 570 respectively, and leads to the approximated expressions

$$\mathfrak{F}_\chi^{(1)}(A_{n,l-1}, \mathfrak{F}_{n,l}) := \mathfrak{F}_\chi(A_{n,l-1}) + D_{\mathbf{B}_p} \mathfrak{F}_\chi(A_{n,l-1})[\mathfrak{F}_{n,l}], \quad (53a)$$

$$\mathfrak{G}^{(1)}(\Theta_{n,l-1}, \mathfrak{F}_{n,l}) := \mathfrak{G}(\Theta_{n,l-1}) + \mathbb{Y}(\Theta_{n,l-1}) : \mathfrak{F}_{n,l}, \quad (53b)$$

571 where $D_{\mathbf{B}_p} \mathfrak{F}_\chi(A_{n,l-1})[\boldsymbol{\Phi}_{n,l}]$ denotes the Gâteaux derivative of \mathfrak{F}_χ , computed at
 572 $A_{n,l-1}$ along the direction of the plastic increment $\boldsymbol{\Phi}_{n,l}$ [19, 93], and $\mathbb{Y}(\Theta_{n,l-1})$
 573 is the fourth-order tensor defined by

$$\mathbb{Y}(\Theta_{n,l-1}) = \frac{\partial \mathcal{G}}{\partial \mathbf{B}_{pn}}(\Theta_{n,l-1}) \in [T\mathbb{C}_R]_2^2. \quad (54)$$

574 Note that $\mathbb{Y}(\Theta_{n,l-1})$ is pair-symmetric, i.e., in its component representation,
 575 it holds that

$$[\mathbb{Y}(\Theta_{n,l-1})]_{CD}^{AB} = [\mathbb{Y}(\Theta_{n,l-1})]_{CD}^{BA}, \quad (55a)$$

$$[\mathbb{Y}(\Theta_{n,l-1})]_{CD}^{AB} = [\mathbb{Y}(\Theta_{n,l-1})]_{DC}^{AB}. \quad (55b)$$

576 We remark that also \mathfrak{F}_p has to be linearised in the same fashion as \mathfrak{F}_χ in
 577 the cases in which it involves \mathbf{B}_{pn} among its arguments (e.g., if the hydraulic
 578 conductivity depends on \mathbf{B}_p).

579 We now set $\mathcal{G}^{(1)}(\Theta_{n,l-1}, \boldsymbol{\Phi}_{n,l}) = \mathbf{0}$, and solve for $\boldsymbol{\Phi}_{n,l}$, thereby obtaining

$$\boldsymbol{\Phi}_{n,l} \equiv \hat{\boldsymbol{\Phi}}(\Theta_{n,l-1}) = -[\mathbb{Y}(\Theta_{n,l-1})]^{-1} : \mathcal{G}(\Theta_{n,l-1}). \quad (56)$$

580 In this way, the increment $\boldsymbol{\Phi}_{n,l}$ is written as a function of χ_n . This allows to
 581 eliminate statically $\boldsymbol{\Phi}_{n,l}$ from $\mathfrak{F}_\chi^{(1)}$. Indeed, by substituting the right-hand-side
 582 of (56) into (53a), we obtain the new functional

$$\tilde{\mathfrak{F}}_\chi^{(2)}(A_{n,l-1}) = \mathfrak{F}_\chi(A_{n,l-1}) - \mathcal{L}(A_{n,l-1}), \quad (57)$$

583 where the auxiliary quantity $\mathcal{L}(A_{n,l-1})$ reads

$$\mathcal{L}(A_{n,l-1}) := D_{\mathbf{B}_p} \mathfrak{F}_\chi(A_{n,l-1}) [[\mathbb{Y}(\Theta_{n,l-1})]^{-1} : \mathcal{G}(\Theta_{n,l-1})]. \quad (58)$$

584 In (56), the inversion of \mathbb{Y} is performed as follows. Let d denote the dimension
 585 of the tangent space $T_X \mathbb{C}_R$ at $X \in \mathbb{C}_R$ (e.g., $d = \dim(T_X \mathbb{C}_R) = 3$). Since \mathbb{Y} is
 586 a fourth-order tensor, it has d^4 components in the representation

$$\mathbb{Y} = Y^{AB}_{CD} \mathbf{E}_A \otimes \mathbf{E}_B \otimes \mathbf{E}^C \otimes \mathbf{E}^D,$$

587 where $\{\mathbf{E}_M\}_{M=1}^d \subset T_X \mathbb{C}_R$ and $\{\mathbf{E}^M\}_{M=1}^d \subset T_X^* \mathbb{C}_R$ are bases of $T_X \mathbb{C}_R$ and
 588 $T_X^* \mathbb{C}_R$, respectively. Now, the set of d^4 scalars $[Y^{AB}_{CD}]$ is identified with a
 589 $d^2 \times d^2$ matrix $[\mathbf{Y}]$, which can be inverted by means of standard methods. In
 590 this work, we used a LU-decomposition. We remark that, due to the spatial dis-
 591 cretisation of the Finite Element Method, this LU-decomposition needs to be
 592 performed at every integration point of an element. The inverse matrix $[\mathbf{Y}^{-1}]$
 593 is thus a representation of the fourth-order tensor \mathbb{Y}^{-1} . Note that, in (56), the
 594 second-order tensor \mathcal{G} is represented as a vector-like column array \mathbf{G} with d^2
 595 entries.

596 Now, for fixed $\mathbf{B}_{pn,l-1}$, with $l \geq 1$, we determine pressure and deformation
 597 by solving iteratively the sub-problem

$$\tilde{\mathfrak{F}}_\chi^{(2)}(A_{n,l-1}) = 0, \quad (59a)$$

$$\tilde{\mathfrak{F}}_p(w_n) = 0. \quad (59b)$$

598 At the k th iteration, $k \geq 1$, we define

$$w_{n,k} := (p_{n,k}, \chi_{n,k}), \quad (60a)$$

$$\Theta_{n,k,l-1} := (\chi_{n,k}, \mathbf{B}_{pn,l-1}), \quad (60b)$$

$$\Lambda_{n,k,l-1} := (p_{n,k}, \chi_{n,k}, \mathbf{B}_{pn,l-1}), \quad (60c)$$

599 and apply a Newton method to (59a) and (59b). That is, we solve the linearised
600 set of equations

$$a(\mathbf{h}_{n,k}, \tilde{\mathbf{u}}) - b(\tilde{\mathbf{u}}, \pi_{n,k}) = -\tilde{\mathfrak{F}}_{\chi}^{(2)}(\Lambda_{n,k-1,l-1}), \quad (61a)$$

$$-c(\mathbf{h}_{n,k}, \tilde{p}) - d(\pi_{n,k}, \tilde{p}) = -\tilde{\mathfrak{F}}_p(w_{n,k-1}). \quad (61b)$$

601 In (61a) and (61b), the bilinear forms $a(\cdot, \cdot)$, $b(\cdot, \cdot)$, $c(\cdot, \cdot)$ and $d(\cdot, \cdot)$ are
602 defined by means of the Gâteaux derivatives of the functionals $\tilde{\mathfrak{F}}_{\chi}^{(2)}$ and $\tilde{\mathfrak{F}}_p$:

$$\begin{aligned} a(\mathbf{h}_{n,k}, \tilde{\mathbf{u}}) &= D_{\chi} \tilde{\mathfrak{F}}_{\chi}^{(2)}(\Lambda_{n,k-1,l-1})[\mathbf{h}_{n,k}] \\ &= \int_{\mathbb{C}_{\mathbb{R}}} \mathbf{g} \text{Grad } \tilde{\mathbf{u}} : \mathbb{A}_{n,k-1,l-1}^{(2)} : \mathbf{H}_{n,k}, \end{aligned} \quad (62a)$$

$$\begin{aligned} -b(\tilde{\mathbf{u}}, \pi_{n,k}) &= D_p \tilde{\mathfrak{F}}_{\chi}^{(2)}(\Lambda_{n,k-1,l-1})[\pi_{n,k}] \\ &= \int_{\mathbb{C}_{\mathbb{R}}} \left\{ -J_{n,k-1} \pi_{n,k} \mathbf{F}_{n,k-1}^{-\text{T}} : \text{Grad } \tilde{\mathbf{u}} \right\}, \end{aligned} \quad (62b)$$

$$\begin{aligned} -c(\mathbf{h}_{n,k}, \tilde{p}) &= D_{\chi} \tilde{\mathfrak{F}}_p(w_{n,k-1})[\mathbf{h}_{n,k}] \\ &= - \int_{\mathbb{C}_{\mathbb{R}}} \{ (\text{Grad } \tilde{p}) [(\mathbb{K}_{n,k-1} : \mathbf{H}_{n,k}) \text{Grad } p_{n,k-1}] \} \\ &\quad - \frac{b(\mathbf{h}_{n,k}, \tilde{p})}{\Delta t_n}, \end{aligned} \quad (62c)$$

$$\begin{aligned} -d(\pi_{n,k}, \tilde{p}) &= D_p \tilde{\mathfrak{F}}_p(w_{n,k-1})[\pi_{n,k}] \\ &= - \int_{\mathbb{C}_{\mathbb{R}}} (\text{Grad } \tilde{p}) [\mathbf{K}_{n,k-1} \text{Grad } \pi_{n,k}], \end{aligned} \quad (62d)$$

603 where $\mathbf{H}_{n,k} = \text{Grad } \mathbf{h}_{n,k}$, and the tensors $\mathbb{A}_{n,k-1,l-1}^{(2)}$, $\mathbb{K}_{n,k-1}$ and $\mathbf{K}_{n,k-1}$ are
604 given by

$$\begin{aligned} \mathbb{A}_{n,k-1,l-1}^{(2)} &= -J_{n,k-1} p_{n,k-1} \mathbf{g}^{-1} \mathbf{F}_{n,k-1}^{-\text{T}} \otimes \mathbf{F}_{n,k-1}^{-\text{T}} \\ &\quad + J_{n,k-1} p_{n,k-1} \mathbf{g}^{-1} \mathbf{F}_{n,k-1}^{-\text{T}} \overline{\otimes} \mathbf{F}_{n,k-1}^{-1} \\ &\quad + (\mathbb{A}_{n,k-1,l-1}^{\text{sc}} - \mathbb{L}_{n,k-1,l-1}), \end{aligned} \quad (63a)$$

$$\mathbb{K}_{n,k-1} = \frac{\partial \hat{\mathbf{K}}}{\partial \mathbf{F}}(\mathbf{F}_{n,k-1}), \quad (63b)$$

$$\mathbf{K}_{n,k-1} = \hat{\mathbf{K}}(\mathbf{F}_{n,k-1}). \quad (63c)$$

605 In particular, $\mathbb{A}_{n,k-1,l-1}^{\text{sc}}$ is the constitutive acoustic tensor computed at the
606 l th iteration in \mathbf{B}_{pn} and at the k th iteration in χ_n , i.e.,

$$\mathbb{A}_{n,k-1,l-1}^{\text{sc}} = \frac{\partial \hat{\mathbf{P}}^{\text{sc}}}{\partial \mathbf{F}}(\mathbf{F}_{n,k-1}, \mathbf{B}_{pn,l-1}), \quad (64)$$

607 while $\mathbb{L}_{n,k-1,l-1}$ is a fictitious acoustic tensor, introduced by the algorithm,
 608 and induced by the Gâteaux derivative of the functional \mathfrak{L} with respect to the
 609 deformation (cf. (58)), i.e.,

$$D_{\chi}\mathfrak{L}(\Lambda_{n,k-1,l-1})[\mathbf{h}_{n,k}] := \int_{\mathbb{C}_R} \mathbf{g} \text{Grad } \tilde{\mathbf{u}} : \mathbb{L}_{n,k-1,l-1} : \mathbf{H}_{n,k}. \quad (65)$$

610 It is important to remark that the effective acoustic tensor

$$(\mathbb{A}_{n,k-1,l-1}^{\text{sc}} - \mathbb{L}_{n,k-1,l-1})$$

611 should be positive definite (cf., for example, [17, 18]). Although our numerical
 612 simulations produced reasonable results, we have not formulated theorems yet,
 613 which predict when this condition fails to be satisfied.

614 The algorithm proposed in this paper requires a linearisation with respect
 615 to χ_n and one with respect to \mathbf{B}_{pn} . Therefore, compared with the classical
 616 RMA [93], an additional linearisation iteration is performed. This increases the
 617 computational effort, but makes our algorithm more flexible and suitable for
 618 various types of remodelling laws, which could also be much more complicated
 619 than the one given in (41).

620 The numerical method presented in this work has been implemented in
 621 UG4, a novel version of the software framework UG (“Unstructured Grids”)[96].
 622 Its algebra, discretisation and grid libraries as well as its massive-parallel
 623 solvers for coupled partial differential equations served as a basis for com-
 624 puting a benchmark problem of the presented poroplastic model.

625 5 Results

626 The unconfined compression test is a very common experimental procedure
 627 that is performed to determine the mechanical and fluid dynamic properties
 628 of hydrated soft tissues, such as articular cartilage [51]. In this benchmark, a
 629 sample of tissue is inserted between two rigid and impermeable parallel plates,
 630 and compressed according to some prescribed loading protocol, which can be
 631 either in force- or in displacement-control. During compression, the parts of
 632 the specimen’s boundary that are not in contact with the plates, and through
 633 which the interstitial fluid can escape, can expand freely.

634 For our simulations, we consider a cylindrical specimen of biphasic material
 635 characterised by initial height $H_0 = 1$ mm and initial radius $R_0 = 1.5$ mm.
 636 The lower boundary of the specimen is clamped at the lower plate of the
 637 experimental apparatus and kept fixed. The upper boundary, instead, is in
 638 contact with the moving plate and is assumed to expand without friction in
 639 axial-symmetric way. Finally, the lateral boundary of the specimen is traction-
 640 free and permeable to fluid flow. The above description of the experiment can
 641 be translated into mathematical formulae as follows: let Γ_l , Γ_L , and Γ_u be
 642 the lower, lateral, and upper boundaries of the specimen in its undeformed

643 configuration (which is taken coincident with the reference configuration), i.e.,
 644 $\partial\mathcal{C}_R = \Gamma_1 \cup \Gamma_L \cup \Gamma_u$. Then, for all $t \in \mathcal{J} \equiv [0, T]$, we prescribe:

$$\text{on } \Gamma_1, \quad \begin{cases} \chi(X, t) = \chi(X, 0) = X \in \Gamma_1, \\ (-\mathbf{K}\text{Grad } p) \cdot \mathbf{N} = 0, \end{cases} \quad (66a)$$

$$\text{on } \Gamma_L, \quad \begin{cases} (-Jp \mathbf{g}^{-1} \mathbf{F}^{-T} + \mathbf{P}_{sc}) \cdot \mathbf{N} = \mathbf{0}, \\ p = 0, \end{cases} \quad (66b)$$

$$\text{on } \Gamma_u, \quad \begin{cases} \chi^z(X, t) = \chi_b^z(t) [\Theta(t) - \Theta(t - T_0)] + \chi_b^z(T_0) \Theta(t - T_0), \\ (-\mathbf{K}\text{Grad } p) \cdot \mathbf{N} = 0, \end{cases} \quad (66c)$$

645 where Θ is the Heaviside function (here defined such that $\Theta(\xi) = 1$, if $\xi \geq 0$,
 646 and $\Theta(\xi) = 0$, if $\xi < 0$), χ_b^z is the axial compressive deformation imposed at
 647 the upper boundary, i.e.,

$$\chi_b^z(t) = H_0/2 - u_T \frac{t}{T_0}, \quad (67)$$

648 $T_0 \in (0, T)$ is the final instant of time of the loading ramp, and $u_T > 0$ is
 649 the target displacement (here, we took $u_T = 0.15$ mm). To observe how the
 650 perturbed system relaxes towards a stationary state, we took $T_0 = 30$ s and
 651 $T = 80$ s. Looking at (66a)–(66c), it is clear that the Dirichlet- and Neumann-
 652 like subsets of $\partial\mathcal{C}_R$ associated with the deformation, Γ_D^X and Γ_N^X , are given by
 653 $\Gamma_D^X = \Gamma_1 \cup \Gamma_u$ and $\Gamma_N^X = \Gamma_L$, respectively, while it holds that $\Gamma_D^p = \Gamma_L$ and
 654 $\Gamma_N^p = \Gamma_1 \cup \Gamma_u$ for the pressure.

655 The material parameters used for this test are reported in Table 1. The
 656 elastic coefficients for the Holmes-Mow strain energy density given in (10a)
 657 are selected in such a way that $\beta = \alpha_1 + 2\alpha_2 = 1$ [57].

Table 1 material parameters

elastic coefficient	α_0	0.125 N/mm ²
elastic coefficient	α_1	0.78
elastic coefficient	α_2	0.11
elastic coefficient	β	1.0
referential hydraulic conductivity	k_{0R}	$3.7729 \cdot 10^{-3} \text{ mm}^4 / (\text{N} \cdot \text{s})$
material parameter	m_0	0.0848
material parameter	m_1	4.638
referential solidity	ϕ_{sR}	0.2
initial yields stress	τ_y	0.002 N/mm ²
coefficient in the plastic flow rule	λ	0.5 mm ² / (N · s)

658 The results of our numerical tests, reported in Figs. 3-5, are plotted on a
 659 section of the specimen containing the symmetry axis.

660 To highlight the influence of the plastic distortions on the mechanical and
 661 fluid dynamic response of the specimen, we compared the radial and axial
 662 components of the fluid filtration velocity, the pressure distribution, and the
 663 first invariant of the constitutive part of the Mandel stress tensor obtained in

664 the poroelastic case (left column of Fig. 3) with those obtained in the presence
 665 of plastic distortions, i.e., in the poroplastic case (right column of Fig. 3). To
 666 characterise the poroelastic case, we simulated an unconfined compression test
 667 in which the yields stress, τ_y , which determines the onset of plastic flow, was
 668 set equal to a value that is never reached by the stress in the tissue. More
 669 precisely, we chose $\tau_y = 2000.00 \text{ N/mm}^2$, a value that led to a purely elastic
 670 material response. In this situation, it holds that $\mathbf{B}_p = \mathbf{G}^{-1}$ at all times of the
 671 observation time interval. In the poroplastic case, instead, \mathbf{B}_p is determined
 672 by means of the numerical procedure reported in Sect. 4. Figures 5(a) and 5(b)
 673 show the first and second invariant of \mathbf{B}_p at the end of the loading ramp, i.e.,
 674 at $t = 30 \text{ s}$. We found that the higher values of these invariants are attained
 675 at the points of the specimen's boundary corresponding to the intersection of
 676 Γ_1 and Γ_L .

677 Before commenting our results, we recall that, in this paper, remodelling
 678 is entirely described in terms of “plastic” distortions. Thus, plotting figures in
 679 which plastic distortions are switched off actually means to show the results
 680 in which no remodelling occurs.

681 Looking at Fig. 3, we notice that the influence of remodelling manifests
 682 itself through the modulation of the fluid filtration velocity, the change of
 683 the pore pressure distribution, and the lowering of the constitutive part of
 684 the stress of the solid phase. In particular, Figs. 3(a) and 3(b) show that the
 685 magnitudes of the radial and the axial filtration velocity, computed according
 686 to Darcy's law, i.e., $\phi_f \mathbf{v}_{fs} = -\mathbf{k} \text{grad} p$, decrease in the poroplastic case. In
 687 Figs. 3(a) and 3(b), the arrows represent the local direction of the flow. The
 688 decrease of the magnitude of the filtration velocity characterising the poro-
 689 plastic case is related to the decrease of the pore pressure (see Fig. 3(c)) and
 690 the decrease of stress, which in Fig. 3(d) is accounted for by the first invariant
 691 of $\boldsymbol{\Sigma}_{sc}$. The values of the first invariant of $\boldsymbol{\Sigma}_{sc}$ are computed with respect to
 692 the reference configuration. However, in a visualisation post-process, the refer-
 693 ence configuration is deformed by the motion map, so that the previously
 694 computed values of the first invariant are visualised in the deformed config-
 695 uration. We remark that the onset and evolution of plastic distortions affect
 696 both quantitatively and qualitatively the time trend of pressure. Indeed, in
 697 Fig. 4, where pressure is evaluated at the midpoint of the lower boundary of
 698 the specimen, one can see that at least three facts distinguish the evolution of
 699 pressure in the poroplastic case (i.e., when remodelling occurs) from that per-
 700 taining the poroelastic one. Firstly, the maximum value of pressure attained
 701 in the absence of remodelling is much higher than the maximum reached in
 702 the presence of remodelling (it should be noticed, however, that in both cases
 703 the maxima are attained at the end of the loading ramp, i.e., at $t = 30 \text{ s}$).
 704 Secondly, the rate with which the pressure tends towards the stationary state
 705 is much higher in the poroplastic case than in the poroelastic one. Thirdly,
 706 pressure seems to be a convex function of time over the interval $[0, T_0]$ in the
 707 poroelastic case, and to become concave in the poroplastic case. A possible
 708 explanation for the change of the pressure's behaviour could be given by the
 709 following argument: The pressure and the deformation are determined by the

710 coupled equations representing the mass and linear momentum balance laws,
 711 i.e., (44a) and (44b). In particular, the balance of momentum (44b) relates the
 712 pressure, p , to the constitutive part of the first Piola-Kirchhoff stress tensor,
 713 \mathbf{P}_{sc} . The plastic distortions, represented by \mathbf{B}_p , have a direct influence on \mathbf{P}_{sc} ,
 714 since it holds that $\mathbf{P}_{\text{sc}} = \hat{\mathbf{P}}_{\text{sc}}(\mathbf{F}, \mathbf{B}_p)$, and, through the balance of momentum,
 715 they also have an indirect influence on p .

716 The coarsest computational grid consists of 144 prismatic elements. A regu-
 717 lar refinement is performed three times, so that the finest grid provides 163300
 718 degrees of freedom for the deformation and the pressure. Both the deforma-
 719 tion, χ , and the pressure, p , are approximated by linear *ansatz* functions. As
 720 a numerical solver a Newton-method is applied. Within the Newton iteration,
 721 a Bi-CGSTAB-method, preconditioned by an ILU-decomposition, solves the
 722 linearised sub-problems. The non-linear convergence is ensured by the appli-
 723 cation of a line-search method.

724 6 Conclusions

725 In this work, we considered a biphasic, solid-fluid mixture as an idealisation of
 726 a biological system, and studied its mechanical and fluid dynamic behaviour
 727 by simulating an unconfined compression test. Our fundamental hypothesis
 728 was that the mechanical loads applied to the mixture, besides leading to a
 729 global change of shape, also induce a structural reorganisation of the solid
 730 phase, which manifests itself through plastic distortions. In order to describe
 731 this physical picture, we used the poroplastic model reported in (44a)–(44c),
 732 which results into a set of coupled, and highly non-linear equations. We recall
 733 that all our calculations have been run under the assumptions that the solid
 734 phase exhibits hyperelastic response and that the fluid obeys Darcy’s law.

735 Equations (44a)–(44c) were solved numerically by applying a numerical
 736 procedure recently developed for monophasic continua [47], and adapted to the
 737 biphasic framework in this paper. The results of our simulations, performed
 738 with our own code, and implemented in the non-commercial software UG [96],
 739 are reported in Sect. 5. It is shown that the plastic distortions, described by \mathbf{B}_p ,
 740 influence the overall deformation, the stress distribution in the medium, and
 741 the fluid filtration velocity. This influence can be observed by comparing the
 742 results obtained in the poroplastic case with those pertaining the poroelastic
 743 one (see Figs. 3(a)–5(b)). We found that the reorganisation of the medium’s
 744 internal structure has repercussions on the magnitudes of both the axial and
 745 the radial component of the Darcy’s filtration velocity, which are smaller in the
 746 poroplastic case than in the poroelastic one, and has the effect of decreasing
 747 the fluid pressure as well as the magnitude of the constitutive stress in the
 748 tissue.

749 Our results could contribute to estimate the mechanical conditions leading
 750 to the onset of remodelling, and seem to suggest some possible consequences
 751 of the structural reorganisation of hydrated soft tissues. Moreover, they may
 752 provide indications about the mechanical conditions regulating the health of

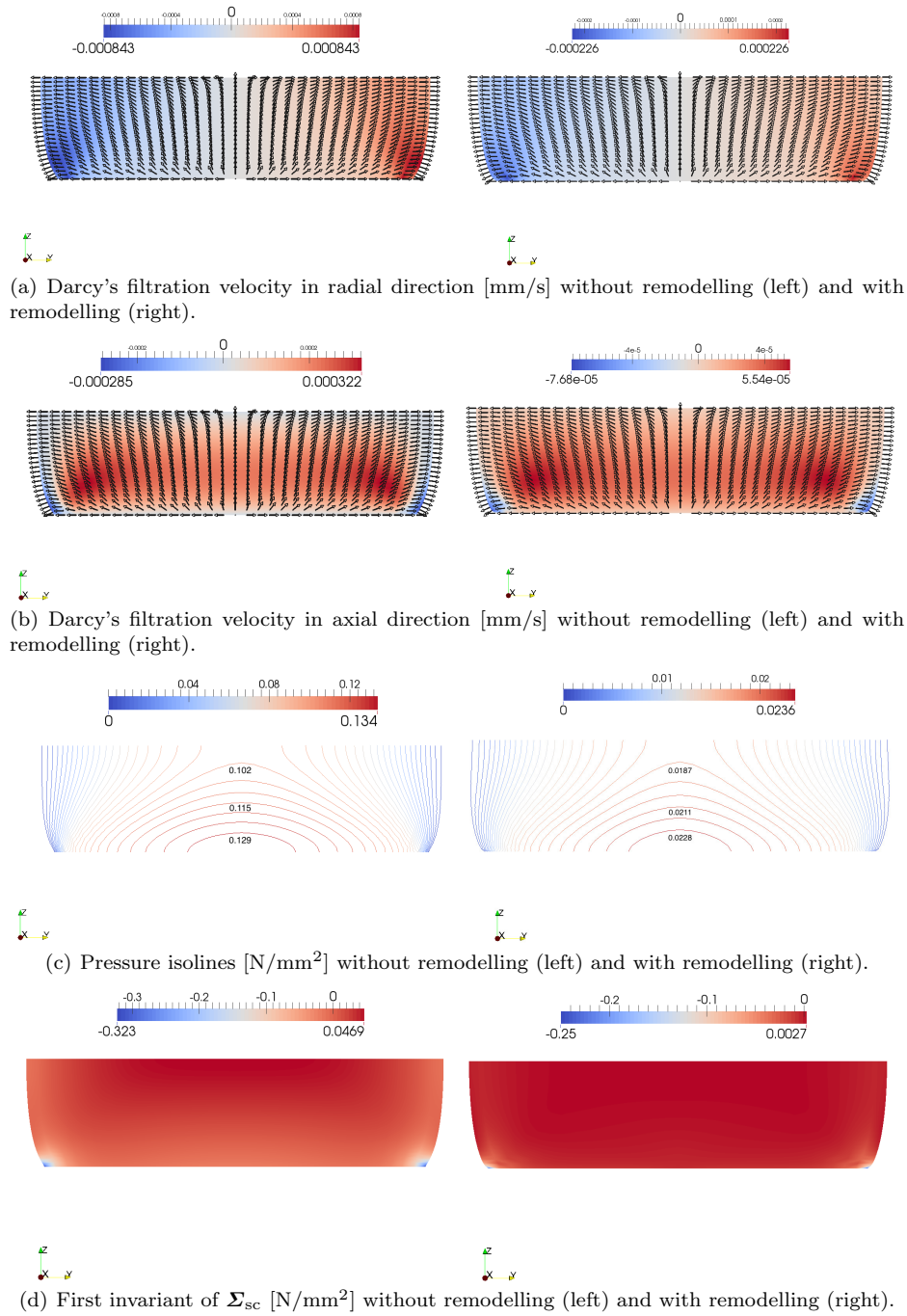


Fig. 3 Comparison of the results of the unconfined compression test in the absence (left column) and in the presence (right column) of remodelling. All quantities are plotted in the deformed configuration of the sample at time $t = 30$ s

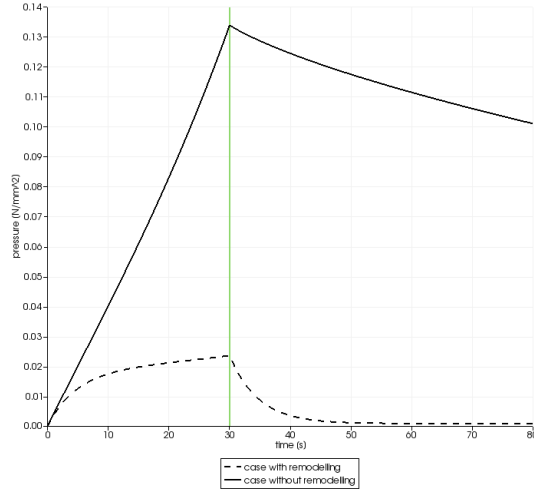


Fig. 4 Comparison of the time evolution of pressure, evaluated at the midpoint of the lower boundary of the sample, between the case without remodelling and the case with remodelling

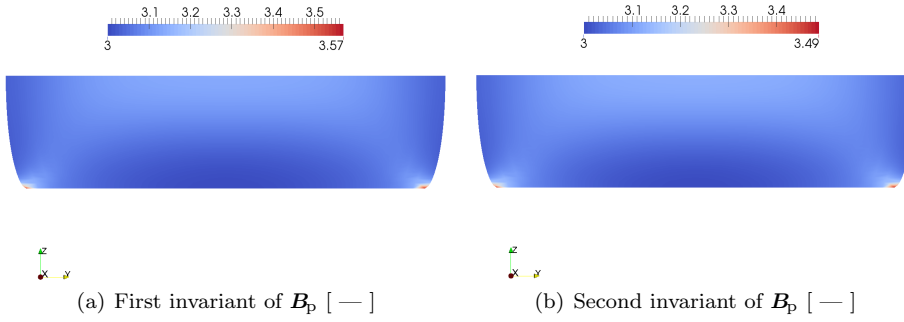


Fig. 5 First and second invariant of \mathbf{B}_p in the presence of remodelling. The invariants are computed at time $t = 30$ s with respect to the reference configuration. However, in a visualisation post-process, the reference configuration is deformed by the motion map, and the invariants are visualised in the deformed configuration.

753 tissues. For example, in the case of articular cartilage, the health of the tissue
 754 depends on the mechanical environment in which chondrocytes live (the
 755 chondrocytes are the cells that synthesise extracellular matrix, cf. [54,55,73,
 756 74] and references therein). Finally, the mathematical model presented in this
 757 paper could be generalised to include also growth [45] and damage [23,24,41].
 758 Indeed, both processes have many features in common with remodelling, and
 759 can be described by extending the BKL decomposition as follows [71]

$$\mathbf{F} = \mathbf{F}_e \mathbf{F}_g \mathbf{F}_p \mathbf{F}_d, \quad (68)$$

760 where \mathbf{F}_g and \mathbf{F}_d denote the tensors of anelastic distortions related to growth
 761 and damage, respectively. A mathematical model based on (68) would require

the introduction of two other independent evolution laws, one for \mathbf{F}_g and one for \mathbf{F}_d , which would call for further adapting the numerical procedure presented in Sect. 4. This is part of our current investigations. We remark that the order with which the tensors \mathbf{F}_g and \mathbf{F}_d appear in (68) is not unique, but it becomes irrelevant if \mathbf{F}_g and \mathbf{F}_d are assumed to be purely volumetric [43].

Equations (44a) and (44b) are rather standard and constitute the starting point for both poroelastic and poroplastic models of solid-fluid mixtures. They are obtained on the basis of a series of assumptions that require: the intrinsic incompressibility of both the solid and the fluid phase, the fluid phase to be macroscopically inviscid (this implying that it can only sustain hydrostatic stresses), the hyperelastic behaviour of the solid phase, and the validity of Darcy’s law. The latter involves the hydraulic conductivity tensor, which was specified in this work by means of the simplest constitutive law for isotropic materials (cf. (29a)). Although many of these hypotheses are physically sound, it could be interesting to investigate the consequences of relaxing some of them. This could lead to more general models that, on the one hand, would stimulate the development of more flexible and efficient computational algorithms, and, on the other hand, might capture some physical aspects (such as, e.g., the pore scale interactions between the solid and the fluid), which are often neglected in the standard theory.

From the computational point of view, assuming that \mathbf{k} is proportional to \mathbf{g}^{-1} introduces the great advantage of weakening the coupling among (44a)–(44c). Indeed, since \mathbf{B}_p does not feature in the mass balance law (44a), the linearisation of the functional \mathfrak{F}_p needs to be performed only with respect to pressure and deformation (we recall that, actually, \mathfrak{F}_p is affine in p , and that the linearisation of \mathfrak{F}_p with respect to the pressure is done to get the set of equations (61a) and (61b), whose algebraic form leads to a “generalised saddle-point problem” [16, 44]). In other circumstances, however, \mathfrak{F}_p has to be linearised according to the same procedure as \mathfrak{F}_χ . This happens, for instance, if the hydraulic conductivity is isotropic, but its constitutive expression is of the type

$$\mathbf{k} = \hat{\mathbf{k}}(\mathbf{F}, \mathbf{B}_p) = k_0 \mathbf{g}^{-1} + k_1 \mathbf{F} \mathbf{B}_p \mathbf{F}^T. \quad (69)$$

In this case, indeed, the coupling among the model equations is due to both χ and \mathbf{B}_p .

The evolution of the plastic distortions depends strongly on the physics of the anelastic phenomenon that has to be described, and, even when the “same” phenomenon is investigated, it can vary considerably depending on the accuracy of the mathematical model, on the strength of the coupling between the rate of anelastic distortions and the other variables, and on the intrinsic features of the anelastic process (which could be either rate-dependent or rate-independent, either associative or non-associative). In this paper, we chose to describe the evolution of \mathbf{B}_p by means of (40) because this plastic flow rule has already been successfully employed in [42] to model the reorganisation of cellular aggregates. Equation (40), however, can be generalised to include a great variety of physical situations.

The major limitation of our model is that it is isotropic and homogeneous. Indeed, both the strain energy density, \tilde{W}_{sk} , and the hydraulic conductivity, \mathbf{k} , are isotropic (see (10a) and (29a)), and all the parameters appearing in their constitutive expressions, including the referential volumetric fraction of the solid phase, ϕ_{sR} , are set equal to constants. If, on the one hand, the model could be acceptable for studying the structural evolution of tumour tissues, which are often assumed to be elastically and hydraulically isotropic [1, 42, 84], it fails to be accurate for tissues, such as articular cartilage, in which the presence of reinforcing collagen fibres induces anisotropy [35, 78, 79, 94], and the constitutive laws are strongly dependent on material points. In these cases, whereas the balance laws (44a) and (44b) only need to account for the contribution of the fibres to the strain energy density and hydraulic conductivity, the plastic flow rule (44c) should be reformulated. Some of our plans for the future include the specification of the numerical techniques put forward in [39, 75] to anisotropic and inhomogeneous porous media.

One of the projects of our future research is to extend the theoretical and computational framework outlined in this paper to models accounting for phase transitions [28], to theories that describe the reorganisation of the internal structure of a body by augmenting its kinematics [21, 27, 45, 50], and to the more general context of biomechanical models of growth and remodelling that involve, among plasticity [80], damage [81], and pre-stress effects [82], also higher order gradients of the deformation [66, 67].

Acknowledgements The authors gratefully acknowledge the Polytechnic of Turin (Italy) [AG and RP], the Goethe Universität Frankfurt (Germany), the German Ministry for Economy and Technology (BMWi) —contract 02E10326 [AG and GW]— and the Baden Württemberg-Stiftung [RP]. AG thanks Melania Carfagna for useful discussions.

References

1. D. Ambrosi, F. Mollica, On the mechanics of a growing tumor, *Int. J. Eng. Sci.*, 40, 1297–1316 (2002)
2. D. Ambrosi, L. Preziosi, On the closure of mass balance models for tumour growth, *Mathematical Models and Methods in Applied Sciences*, 12(5), 737–754 (2002)
3. D. Ambrosi, L. Preziosi, G. Vitale, The insight of mixtures theory for growth and remodeling, *Z. Angew. Math. Phys.*, 61, 177–191 (2010)
4. D. Ambrosi, L. Preziosi, G. Vitale, The interplay between stress and growth in solid tumors, *Mechanics Research Communications*, 42, 87–91 (2012)
5. U. Andreaus, M. Colloca, D. Iacoviello, M. Pignataro, Optimal-tuning PID control of adaptive materials for structural efficiency, *Struct. Multidiscip. O.*, 43(1), 43–59 (2011)
6. U. Andreaus, M. Colloca, D. Iacoviello, An optimal control procedure for bone adaptation under mechanical stimulus, *Control Eng. Pract.*, 20, 575–583 (2012)
7. U. Andreaus, M. Colloca, D. Iacoviello, Modelling of trabecular architecture as result of an optimal control procedure. In: *Biomedical Imaging and Computational Modeling in Biomechanics*, Iacoviello D. and Andreaus U. (Eds.), Chapter II, pp. 19–37. Springer, Dordrecht, (2012)
8. U. Andreaus, M. Colloca, D. Iacoviello, Optimal bone density distributions: Numerical analysis of the osteocyte spatial influence in bone remodeling, *Comput. Methods Programs Biomed.*, 113(1), 80–91 (2014)

- 852 9. U. Andreaus, I. Giorgio, T. Lekszycki, A 2-D continuum model of a mixture of bone tissue
853 and bio-resorbable material for simulating mass density redistribution under load slowly
854 variable in time, *J. Appl. Math. Mech.*, 8, 1–23 (2013), DOI:10.1002/zamm.201200182
- 855 10. U. Andreaus, I. Giorgio, A. Madeo, The influence of different loads on the remodel-
856 ing process of a bone and bioresorbable material mixture with voids, *Continuum Mech.*
857 *Thermodyn.*, Published online: 11 December 2014, DOI: 10.1007/s00161-014-0397-y
- 858 11. U. Andreaus, I. Giorgio, A. Madeo, Modeling of the interaction between bone tissue
859 and resorbable biomaterial as linear elastic materials with voids, *Z. Angew. Math. Phys.*,
860 66(1), 209–237 (2015)
- 861 12. G.A. Ateshian, On the Theory of Reactive Mixtures for Modeling Biological Growth,
862 *Biomech. Model. Mechanobiol.*, 6(6), 423–445 (2007)
- 863 13. G.A. Ateshian, J.A. Weiss, Anisotropic hydraulic permeability under finite deformation,
864 *Journal of Biomedical Engineering*, 132, 111004-111004-7 (2010)
- 865 14. J. Bear, *Dynamics of Fluids in Porous Media*, Dover Publications Inc., New York (1972)
- 866 15. L.S. Bennethum, M.A. Murad, J.H. Cushman, Macroscale thermodynamics and the
867 chemical potential for swelling porous media, *Transport in Porous Media*, 39, 187–225
868 (2000)
- 869 16. A. Benzi, G.H. Golub, J. Liesen, Numerical solution of saddle point problems, *Acta*
870 *Numerica*, 14, 1–137 (2005)
- 871 17. D. Bigoni, D. Zaccaria, Strong ellipticity of comparison solids in elastoplasticity with
872 volumetric non-associativity, *Int. J. Solid Structures*, 29(17), 2123–2136 (1992)
- 873 18. D. Bigoni, D. Zaccaria, On the eigenvalues of the acoustic tensor in elastoplasticity,
874 *European Journal of Mechanics A/Solids*, 13(5), 621–638 (1994)
- 875 19. J. Bonet, R.D. Wood, *Nonlinear Continuum Mechanics for Finite Element Analysis*,
876 Cambridge University Press, Cambridge, New York (2008)
- 877 20. R.M. Bowen, Compressible porous media models by use of the theory of mixtures,
878 *International Journal of Engineering Science*, 20, 697–735, (1982)
- 879 21. P. Cermelli, E. Fried, S. Sellers, Configurational stress, yield and flow in rate-
880 independent plasticity, *Proc R Soc A*, 457, 1447–1467 (2001)
- 881 22. S. Cleja-Tigoiu, G.A. Maugin, Eshelby’s stress tensors in finite elastoplasticity, *Acta*
882 *Mech.*, 139, 231–249 (2000)
- 883 23. L. Contrafatto, M. Cuomo. A new thermodynamically consistent continuum model for
884 hardening plasticity coupled with damage, *Int J Sol Struct*, 39, 6241–6271 (2002)
- 885 24. M. Cuomo, L. Contrafatto, Stress rate formulation for elastoplastic models with internal
886 variables based on augmented Lagrangian regularisation, *Int J Sol Struct*, 37, 3935–3964
887 (2000)
- 888 25. G. Del Bufalo, L. Placidi, M. Porfiri, A mixture theory framework for modeling the
889 mechanical actuation of ionic polymer metal composites, *Smart Materials and Structures*,
890 17(4), 1–17, ISSN: 0964-1726, doi: 10.1088/0964-1726/17/4/045010
- 891 26. F. dell’Isola, L. Rosa, C. Woźniak, Dynamics of solids with micro periodic nonconnected
892 fluid inclusions, *Archive of Applied Mechanics*, 67, 215–228 (1997)
- 893 27. A. DiCarlo, S. Quiligotti, Growth and balance, *Mechanics Research Communications*,
894 29, 449–456 (2002)
- 895 28. V. Emerenyeve, W. Pietraszkiewicz, The nonlinear theory of elastic shells with phase
896 transitions, *Journal of Elasticity*, 85(2), 67–86 (2004)
- 897 29. M. Epstein, *The Geometric Language of Continuum Mechanics*. Cambridge: Cambridge
898 University Press (2010)
- 899 30. M. Epstein, G.A. Maugin, The energy-momentum tensor and material uniformity in
900 finite elasticity, *Acta Mechanica*, 83, 127–133 (1990)
- 901 31. M. Epstein, G.A. Maugin, Thermomechanics of volumetric growth in uniform bodies,
902 *Int. J. Plasticity*, 16, 951–978 (2000)
- 903 32. R.A. Eve, B.D. Reddy, The variational formulation and solution of problems of finite-
904 strain elastoplasticity based on the use of a dissipation function. *Int. J. Numer. Meth.*
905 *Engng.*, 37, 1673–1695 (1994)
- 906 33. S. Federico, Covariant Formulation of the Tensor Algebra of Non-Linear Elasticity. *Int*
907 *J Nonlin Mech*, 47, 273–284 (2012)
- 908 34. S. Federico, Porous Materials with Statistically Oriented Reinforcing Fibres. In: *Non-*
909 *linear Mechanics of Soft Fibrous Materials (CISM Courses and Lectures No. 559, Interna-*
910 *tional Centre for Mechanical Sciences)*, L. Dorfmann and R.W. Ogden (Eds.), Springer,
911 Berling, pp. 49–120 (2015)

- 912 35. S. Federico, A. Grillo, Elasticity and permeability of porous fibre-reinforced materials
913 under large deformations, *Mechanics of Materials*, 44, 58–71 (2012)
- 914 36. S. Federico, W. Herzog, On the permeability of fibre-reinforced porous materials, *Int.*
915 *J. Solids Struc.*, 45, 2160–2172 (2008)
- 916 37. S. Federico, W. Herzog, On the Anisotropy and Inhomogeneity of Permeability in Ar-
917 ticular Cartilage, *Biomech Model Mechanobiol*, 7, 367–378 (2008)
- 918 38. L. Fusi, A. Farina, D. Ambrosi, Mathematical modelling of a solid-liquid mixture with
919 mass exchange between constituents, *Math. Mech. Solids*, 11, 575–595 (2006).
- 920 39. G. Gabriel, K.-J. Bathe. Some Computational Issues in Large Strain Elasto-Plastic
921 Analysis, *Computers and Structures*, 56(2/3), 249–267 (1995)
- 922 40. J.-F. Ganghoffer, On Eshelby tensors in the context of the thermodynamics of open
923 systems: Application to volumetric growth, 48(12), 2081–2098 (2010)
- 924 41. T.C. Gasser, An irreversible constitutive model for fibrous soft biological tissue: A 3-D
925 microfiber approach with demonstrative application to abdominal aortic aneurysms. *Acta*
926 *Biomater*, 7, 2457–2466 (2011)
- 927 42. C. Giverso, L. Preziosi, Modelling the compression and reorganization of cell aggregates.
928 *Math. Med. Biol.*, 29, 181–204 (2012)
- 929 43. C. Giverso, M. Scianna, A. Grillo, Growing avascular tumours as elasto-plastic bodies
930 by the theory of evolving natural configurations, *Mechanics Research Communications*,
931 <http://dx.doi.org/10.1016/j.mechrescom.2015.04.004>. In press.
- 932 44. A. Grillo, C. Giverso, M. Favino, R. Krause, M. Lampe, G. Wittum, Mass Transport in
933 Porous Media with Variable Mass. In: *Numerical Analysis of Heat and Mass Transfer in*
934 *Porous Media, Advanced Structured Materials 27*, Delgado JMPQ et al. (Eds.), Springer,
935 Berlin, Heidelberg (2012).
- 936 45. A. Grillo, S. Federico, G. Wittum, Growth, mass transfer and remodeling in fiber-
937 reinforced, multi-constituent materials, *Int J Nonlin Mech*, 47, 388–401 (2012)
- 938 46. A. Grillo, A. Guaily, C. Giverso, S. Federico, Non-linear model for compression tests
939 on articular cartilage, *Journal of Biomechanical Engineering*, doi: 10.1115/1.4030310. In
940 press.
- 941 47. A. Grillo, R.-A. Prohl, G. Wittum, A generalised algorithm for anelastic processes in
942 elastoplasticity and biomechanics. *Mathematics and Mechanics of Solids*. (Accepted)
- 943 48. A. Grillo, S. Federico, G. Wittum, G. Giaquinta, S. Imatani, M.V. Mićunović, Evolution
944 of a fiber-reinforced mixture, *Nuovo Cimento C*, 32(1), 97–119 (2009).
- 945 49. A. Grillo, G. Wittum, G. Giaquinta, M.V. Mićunović, A multiscale analysis of growth
946 and diffusion dynamics in biological mixtures, *International Journal of Engineering Sci-*
947 *ence*, 47, 261–283 (2009)
- 948 50. A. Grillo, G. Wittum, A. Tomic, S. Federico, Remodelling in statistically oriented fibre-
949 reinforced materials and biological tissues, *Mathematics and Mechanics of Solids*, DOI:
950 10.1177/1081286513515265.
- 951 51. F. Guilak, A. Ratcliffe, V.C. Mow, Chondrocyte deformation and local tissue strain-
952 ing articular cartilage: A confocal microscopy study, *Journal of Orthopaedic Research*,
953 13(3):410-421 (1995).
- 954 52. A. Guillou, R.W. Ogden, Growth in soft biological tissue and residual stress develop-
955 ment, in: G.A. Holzapfel, R.W. Ogden (Eds.), *Mechanics of Biological Tissue*, Springer,
956 Berlin, Heidelberg, 2006.
- 957 53. K. Hackl, F.D. Fischer, On the relation between the principle of maximum dissipation
958 and inelastic evolution given by dissipation potentials, *Proc. R. Soc. A*, 464, 117–132
959 (2008).
- 960 54. S.-K. Han, S. Federico, A. Grillo, G. Giaquinta, W. Herzog, The mechanical behaviour
961 of chondrocytes predicted with a micro-structural model of articular cartilage, *Biomech.*
962 *Model. Mechanobiol.*, 6(3), 139–150 (2007)
- 963 55. S.-K. Han, S. Federico, W. Herzog, A Depth-Dependent Model of the Pericel-
964 lular Microenvironment of Chondrocytes in Articular Cartilage, *Computer Meth-*
965 *ods in Biomechanics and Biomedical Engineering*, 14 (7), 657–664 (2010), DOI:
966 10.1080/10255842.2010.493512
- 967 56. M.S. Hassanizadeh, Derivation of basic equations of mass transport in porous media.
968 Part II. Generalized Darcy’s and Fick’s Laws, *Advances in Water Resources*, 9, 208–222
969 (1986)

- 970 57. M.H. Holmes, V.C. Mow, The nonlinear characteristics of soft gels and hydrated con-
971 nective tissues in ultrafiltration, *Journal of Biomechanics*, 23(11), 1145–1156 (1990).
- 972 58. G.A. Holzapfel, T.C. Gasser, R.W. Ogden, A new constitutive framework for arterial
973 wall mechanics and a comparative study of material models, *Journal of Elasticity*, 61, 1–48
974 (2000)
- 975 59. T.J.R. Hughes, *The finite element method: Linear static and dynamic finite element*
976 *analysis*, Dover, New York, (2000)
- 977 60. T. Lekszycki, F. dell’Isola, A mixture model with evolving mass densities for describing
978 synthesis and resorption phenomena in bones reconstructed with bio-resorbable materials,
979 *ZAMM – Journal of Applied Mathematics and Mechanics / Zeitschrift für Angewandte*
980 *Mathematik und Mechanik*, 6(92), 426–444 (2012)
- 981 61. Y. Liu, H. Zhang, Y. Zheng, S. Zhang, B. Chen, A nonlinear finite element model of
982 the stress analysis of soft solids with a growing mass, *Int. J. Solids Struct*, 51(17), 24,
983 2964–2978 (2014)
- 984 62. B. Loret, F.M.F. Simões, A framework for deformation, generalized diffusion, mass
985 transfer and growth in multi-species multi-phase biological tissues, *European Journal of*
986 *Mechanics A/Solids* 24, 757–781 (2005)
- 987 63. V.A. Lubarda, A. Hoger, On the mechanics of solids with a growing mass, *International*
988 *Journal of Solids and Structures* 39, 4627–4664 (2002)
- 989 64. V.A. Lubarda, Constitutive theories based on the multiplicative decomposition of defor-
990 mation gradient: Thermoelasticity, elastoplasticity, and biomechanics, *Appl. Mech. Rev.*,
991 57(2), 95–108 (2004)
- 992 65. J. Lubliner, *Plasticity Theory*, Dover Publications, Inc., Mineola, New York (2008)
- 993 66. A. Madeo, T. Lekszycki, F. dell’Isola, A continuum model for the biomechanical inter-
994 actions between living tissue and bio-resorbable graft after bone reconstructive surgery,
995 *CR Mecanique*, 339, 625–640 (2011)
- 996 67. A. Madeo, F. dell’Isola, F. Darve, A continuum model for deformable, second gradient
997 porous media partially saturated with compressible fluids. *J Mech Phys Sol*, 61, 2196–2211
998 (2013)
- 999 68. J.E. Marsden, T.J.R. Hughes, *Mathematical Foundations of Elasticity*, Dover Publica-
1000 tions Inc., New York (1983)
- 1001 69. G.A. Maugin, M. Epstein, Geometrical Material Structure of Elastoplasticity, *Internation-*
1002 *al Journal of Plasticity*, 14(1-3), 109–115 (1998)
- 1003 70. A. Menzel, A fibre reorientation model for orthotropic multiplicative growth. Configu-
1004 rational driving stresses, kinematics-based reorientation and algorithmic aspects. *Biome-*
1005 *chanics and Modeling Mechanobiology*, 6(5), 303–320 (2007)
- 1006 71. M.V. Mićunović, *Thermomechanics of viscoplasticity—fundamentals and applications*.
1007 Springer, Heidelberg (2009)
- 1008 72. Minozzi, M., Nardinocchi, P., Teresi, L., Varano, V.: Growth-induced compatible strains.
1009 *Math. Mech. Solids* (2015). doi: 10.1177/1081286515570510.
- 1010 73. E.K. Moo, W. Herzog, S.-K. Han, N.A. Abu Osman, B. Pinguan-Murphy, S. Federico,
1011 *Mechanical Behaviour of In-Situ Chondrocytes Subjected to Different Loading Rates: A*
1012 *Finite Element Study, Biomechanics and Modeling in Mechanobiology*, 11(7), 983–993
1013 (2012) DOI: 10.1007/s10237-011-0367-2
- 1014 74. E.K. Moo, S.-K. Han, S. Federico, A. Jinha, S. Sibole, N.A. Abu Osman, B. Pinguan-
1015 Murphy, W. Herzog, Extracellular Matrix Integrity Affects the Mechanics of In-Situ Chon-
1016 drocytes under Compression, *Journal of Biomechanics*, 47(5), 1004–1013 (2014) DOI:
1017 10.1016/j.jbiomech.2014.01.003
- 1018 75. F.J. Montáns, K.-J. Bathe, Computational issues in large strain elasto-plasticity: an al-
1019 gorithm for mixed hardening and plastic spin. *International Journal of Numerical Methods*
1020 *in Engineering*, 63, 159–196 (2005)
- 1021 76. B. Nedjar, On finite strain poroplasticity with reversible and irreversible porosity laws.
1022 Formulation and computational aspects, *Mechanics of Materials*, 68, 237–252 (2014)
- 1023 77. T. Olsson, A. Klarbring, Residual stresses in soft tissue as a consequence of growth
1024 and remodelling: Application to an arterial geometry, *European Journal of Mechanics*
1025 *A/Solids*, 27, 959–974 (2008)
- 1026 78. D.M. Pierce, T. Ricken, G.A. Holzapfel, A hyperelastic biphasic fibre-reinforced model
1027 of articular cartilage considering distributed collagen fibre orientations: continuum basis,

- 1028 computational aspects and applications, *Comput. Methods Biomech. Biomed. Eng.*, 16,
1029 1344–1361 (2013)
- 1030 79. D.M. Pierce, T. Ricken, G.A. Holzapfel, Modeling sample/patient-specific structural
1031 and diffusional responses of cartilage using DT-MRI. *Int J Numer Methods Biomed Eng*,
1032 29, 807–821 (2013)
- 1033 80. L. Placidi, A variational approach for a nonlinear one-dimensional damage-elasto-plastic
1034 second-gradient continuum model, *Continuum Mechanics and Thermodynamics*, ISSN:
1035 0935-1175, doi: 10.1007/s00161-014-0405-2 (In press)
- 1036 81. L. Placidi, A variational approach for a nonlinear 1-dimensional second gradient contin-
1037 uum damage model, *Continuum Mechanics and Thermodynamics*, 1–16, ISSN: 0935-1175,
1038 doi: 10.1007/s00161-14-0338-9 (2014)
- 1039 82. L. Placidi, F. dell’Isola, N. Ianiro, G. Sciarra, Variational formulation of pre-stressed
1040 solid-fluid mixture theory, with an application to wave phenomena, *European Journal of*
1041 *Mechanics, A/Solids*, 27(4), 582–606 (2008)
- 1042 83. S. Preston, E. Elżanowski, Material uniformity and the concept of the stress space. In:
1043 *Continuous Media with Microstructure*, 91–101, Springer, Heidelberg (2010)
- 1044 84. L. Preziosi, D. Ambrosi, C. Verdier, An elasto-visco-plastic model of cell aggregates,
1045 *Journal of Theoretical Biology*, 262(1), 35–47 (2010)
- 1046 85. L. Preziosi, A. Farina, On Darcy’s law for growing porous media, *International Journal*
1047 *of Non-Linear Mechanics*, 37(3), 485–491 (2002)
- 1048 86. L. Preziosi, G. Vitale, A multiphase model of tumour ad tissue growth including cell ad-
1049 hesions and plastic reorganization, *Mathematical Models and Methods in Applied Science*,
1050 21, 1901–1932 (2011)
- 1051 87. S. Quiligotti, On bulk growth mechanics of solid-fluid mixtures: kinematics and invari-
1052 ance requirements, *Theor. Appl. Mech. TEOPM7*, 28, 1–11 (2002)
- 1053 88. S. Quiligotti, G.A. Maugin, F. dell’Isola, An Eshelbian approach to the nonlinear me-
1054 chanics of constrained solid-fluid mixtures. *Acta Mechanica*, 160, 45–60, (2003)
- 1055 89. K.R. Rajagopal, Multiple configurations in continuum mechanics, *Rep. Inst. Comput.*
1056 *Appl. Mech*, 6 (1995)
- 1057 90. E.K. Rodriguez, A. Hoger, A.D. McCulloch, Stress-dependent finite growth in soft elas-
1058 tic tissues, *Journal of Biomechanics*, 27, 455–467 (1994)
- 1059 91. G. Sciarra, F. dell’Isola, K. Hutter, Dilatational and compacting behavior around a
1060 cylindrical cavern leached out in a solid-fluid elastic rock salt, *International Journal of*
1061 *Geomechanics*, 5(3), 233–243 (2005)
- 1062 92. J.C. Simo, A framework for finite strain elastoplasticity based on maximum plastic dis-
1063 sipation and the multiplicative decomposition: Part I. *Continuum Formulation*, *Comput.*
1064 *Mech. Appl. M.*, 66, 199–219 (1988).
- 1065 93. J.C. Simo, T.J.R. Hughes, *Computational Plasticity*, Springer, New York (1988)
- 1066 94. A. Tomic, A. Grillo, S. Federico, Poroelastic materials reinforced by statistically oriented
1067 fibres—numerical implementation and application to articular cartilage. *IMA Journal of*
1068 *Applied Mathematics*, 79(5), 1017–1059 (2014) DOI:10.1093/imamat/hxu039.
- 1069 95. C. Truesdell, W. Noll, *The Non-Linear Field Theories of Mechanics*, *Handuch der*
1070 *Physik*, III/3, Berlin: Ed. S. Flugge. Springer-Verlag.
- 1071 96. A. Vogel, S. Reiter, M. Rupp, A. Nägel, G. Wittum, UG4 - A Novel Flexible Software
1072 System for Simulating PDE Based Models on High Performance Computers, *Computing*
1073 *and Visualization in Science*, DOI: 10.1007/s00791-014-0232-9 (2013)